communications earth & environment

Review article

A Nature Portfolio journal

https://doi.org/10.1038/s43247-025-02839-4

Iron's irony: speciation, complexation & microbial processing of Fe in hydrothermal plumes

Solveig I. Bühring [1] ✉, Stefanie Böhnke-Brandt [2], Alexander Diehl [1], Martha Gledhill [2], Laura Haffert [2], Charlotte Kleint [1], Andrea Koschinsky [3], Sinikka Lennartz [4], Mirjam Perner [2], Sylvia G. Sander [2,5], Christoph Völker [6] & Ying Ye [6]

This review integrates vent fluid chemistry and biogeochemical processes to assess how hydrothermal systems influence oceanic iron distribution. Despite rapid precipitation of iron-bearing minerals immediately after venting, buoyant hydrothermal plumes disperse dissolved and nanoparticulate iron across thousands of kilometers, aided by slow oxidation, reversible exchanges between soluble and particulate iron, and biological interactions. These mechanisms underscore hydrothermal vents as a widespread iron source, impacting deep and surface marine ecosystems. Transport dynamics are governed by temperature, pH, microbial activity, and water-mass residence times. We investigate the controls on hydrothermal iron distribution by examining relationships between iron and pH, temperature, chlorinity and hydrogen sulfide in vent fluids, along with solubility modeling of iron(III) hydroxide and iron(II) sulfide. Finally, we highlight key research frontiers that will advance understanding of both hydrothermal processes and their role in shaping the ocean iron biogeochemical cycle.

Iron (Fe) plays a pivotal role in ocean ecosystems by supporting Earth's primary production as an important micronutrient[1,2]. Fe is crucial as a co-factor in enzymatic processes, particularly within photosynthesis, respiration, and nitrogen fixation (e.g., ref. 3). This Fe dependence originates from Earth's early history. Fe is one of the most abundant chemical elements on Earth and when phytoplankton evolved in the Archean anoxic ocean, Fe was present in its highly soluble form, i.e., ferrous Fe (Fe^{2+}). However, in today's ocean, in the presence of oxygen and a slightly alkaline pH, Fe^{2+} is scarce because of its rapid oxidation to ferric iron (Fe^{3+}) and the subsequent formation of barely soluble (oxy)hydroxides. The concentration of Fe^{3+} in natural seawater under these conditions is as low as 10^{-9}–10^{-11} mol L^{-1}, depending on its speciation[4], which clearly makes its biological acquisition a considerable challenge and has important consequences, especially for phytoplankton photosynthesis as a global regulator of the Earth's climate. Throughout the evolution of oxygenic photosynthesis, life itself gradually made biologically essential Fe a "trace element"—which is the enduring irony of iron.

Already in the 1930s, researchers acknowledged that, even in summer when there is abundant light, phytoplankton production is lower than what could be supported by the available nutrients in large areas of the Southern Ocean[5–7]. However, it took almost half a century until the development of trace-metal clean sampling and analysis protocols allowed for the first time to see the real Fe concentration in seawater without the previously associated contamination[8]. The "iron hypothesis" was formulated by John Martin in the late 1980s, after conjecturing that the increased dust-derived Fe delivery to the Southern Ocean during glacial periods led to enhanced utilization of the major nutrients and a corresponding draw-down of atmospheric carbon dioxide[9,10]. Since then, numerous mesoscale Fe fertilization experiments[11,12] and innumerable in-situ process and laboratory studies have been conducted. These experiments and studies show and recognize the importance of Fe in primary production and link its availability to global climate[13–15]. For many years, the Fe-rich eolian dust input was considered to be the major external source of Fe to the ocean (e.g., refs. 16–19). In recent years, especially within the global program GEOTRACES the distribution of trace elements, like Fe, was systematically documented in the world's oceans (e.g., ref. 20). The results from this program helped to identify multiple thus far underestimated sources of Fe to the ocean, such as hydrothermal activity along mid-ocean ridges in the Southern[21], Arctic[22], as well as in the Atlantic[23]

[1]MARUM – Center for Marine Environmental Sciences, University of Bremen, Bremen, Germany. [2]GEOMAR, Helmholtz Centre for Ocean Research Kiel, Kiel, Germany. [3]School of Science, Constructor University Bremen, Bremen, Germany. [4]Institute for Chemistry and Biology of the Marine Environment, Carl von Ossietzky University Oldenburg, Oldenburg, Germany. [5]Faculty of Mathematics and Natural Sciences, Kiel University, Kiel, Germany. [6]Alfred-Wegener-Institut Helmholtz-Zentrum für Polar- und Meeresforschung, Bremerhaven, Germany. ✉e-mail: sbuehring@marum.de

and Pacific[24] oceans, allowing a distinction between the dominance of dust-borne Fe at low latitudes and the increasingly recognized importance of hydrothermal Fe especially for higher latitude regions[23,25–27], where there is increasing evidence for the crucial role of hydrothermal Fe for primary production in the upper ocean (e.g., refs. 28,29). Estimates of hydrothermal Fe derived from vent fluid compositions and hydrothermal fluid mass fluxes range from 19 to 230 Gmol Fe yr^{-1}[30], and concentrations of Fe in the deep ocean can only be reproduced in ocean biogeochemistry models if hydrothermal sources are included[25]. Hydrothermal sources are thus comparable to estimates made for other Fe sources generally considered important to the oceanic Fe budget, i.e., 34–110 Gmol yr^{-1} from reducing sediments[31–33], 1.4–7.0 Gmol yr^{-1} from eolian dust deposition[34,35] and 2–25 Gmol Fe yr^{-1} from rivers[36,37].

In contrast to hydrothermal Fe flux estimates from vent fluids, the Fe flux estimate from hydrothermal sources in ocean biogeochemical models is computed to be in the order of 0.3–0.9 Gmol Fe yr^{-1} globally[25,38]. This flux estimate is 100–1000 times smaller than that expected from vent fluid compositions and points to the importance of mineral precipitation (e.g., Fe-sulfides, Fe-oxyhydroxides) during near-field hydrothermal plume processes significantly reducing the far-field hydrothermal input into the ocean. Nevertheless, hydrothermal Fe is a major source of Fe to the deep ocean, together with non-reductive dissolution of particulate Fe[39,40] and the release of Fe from the remineralization of sinking organic particles, it is thus one of the main mechanisms that can counteract the long-term loss of Fe that occurs via scavenging[24]. If further stabilized and transported to the surface ocean, the potential enhancement of the deep ocean Fe inventory via hydrothermalism will influence the supply ratio of N:Fe to surface waters, which is a critical factor in determining the limiting nutrient at the ocean surface[15].

Most of hydrothermally delivered dissolved Fe precipitates near vents, and formerly it was believed that only negligible amounts escape the vicinity of hydrothermal vent fields[41]. However, we know now that plumes enriched with both colloidal (functionally defined as 0.02–0.2 µm, Fig. 1) and soluble (<0.02 µm) Fe, i.e., above background seawater concentrations, can be transported 1000 s of kilometers away from their source (e.g., refs. 24,42–44), and this has led to a re-evaluation of the hydrothermal input to the oceanic Fe inventory. The formation of authigenic Fe hydroxides[45], the unknown interplay with Fe-bearing inorganic nanoparticles[42,46–48], and the presence of Fe-complexing organic ligands (e.g., ref. 49) are thought to determine this long-distance transport of hydrothermal Fe[42]. The nature of dissolved Fe-binding ligands in seawater is not well constrained, though it has been established that they are widespread in the oceans and variable in Fe binding strength[50]. Siderophores, exopolysaccharides, viral lysis products, and humic substances are only a few examples of organic matter that have been shown to bind Fe in seawater[50]. The number of molecules with Fe-binding capability may be very large (on the order of a few hundred thousand[51]), with the total concentration of binding sites that can bind cations on the order of 1.2–1.5 mmol mol^{-1}[52,53]. Biogeochemical modeling indicates that binding of Fe to organic matter can increase Fe solubility and thus facilitate (long-range) Fe transport away from point sources, like hydrothermal vents, provided the formation of authigenic Fe hydroxides is not favorable[45].

Recent syntheses have highlighted the significance of hydrothermal Fe fluxes to the ocean. German et al.[2] provided a comprehensive review of hydrothermal processes and their contribution to the deep-ocean Fe inventory, while emphasizing that the mechanistic controls on Fe speciation, nanoparticle formation, organic complexation, and microbial transformations remain poorly constrained. Here, we address this gap by

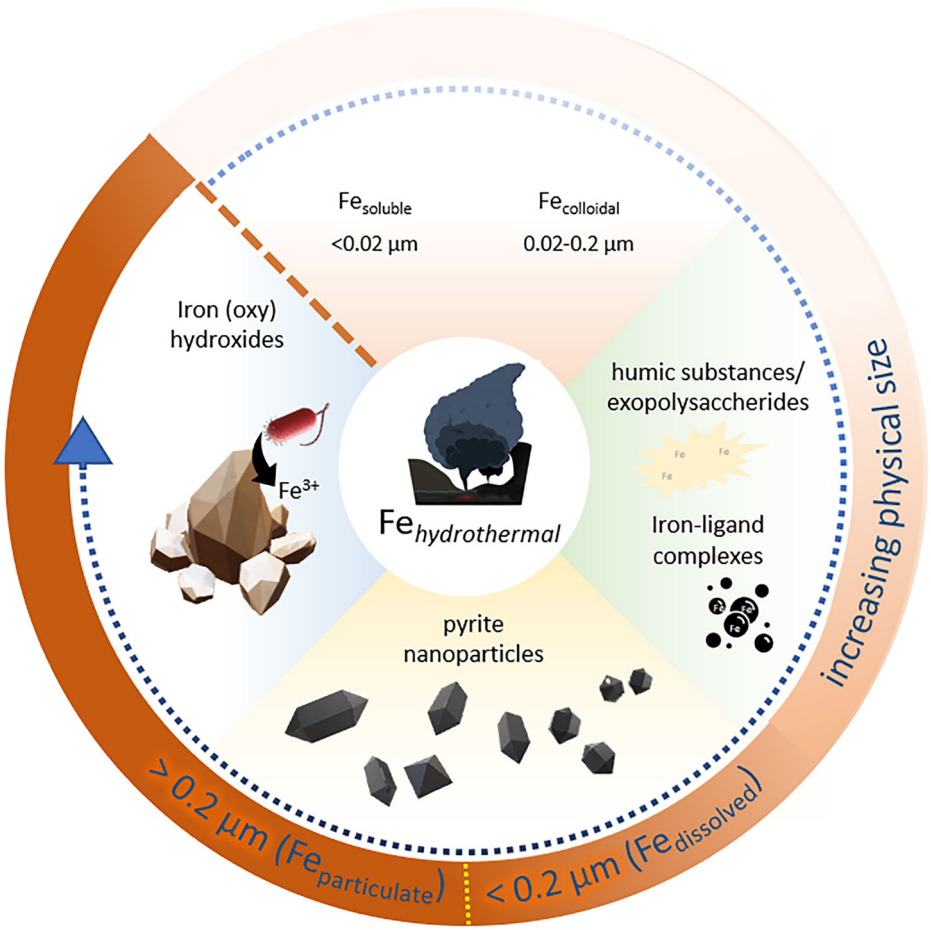

Fig. 1 | Fe species. Chemical Fe speciation and size fractionation in hydrothermal fluids and plumes.

integrating vent fluid chemistry, nanoparticulate Fe phases, organic ligand interactions, and microbial processes into a unified framework for understanding the role of hydrothermal Fe in the ocean. We will review current knowledge about the impact of hydrothermal systems on the distribution of Fe in the ocean and their potential role in influencing marine biological productivity. To that end, we draw on a recently compiled database on hydrothermal vent fluid compositions[54,55] to evaluate the factors that exert a major influence on Fe concentrations in hydrothermal vent fluids, review the biogeochemical processes that influence near field lowering in Fe concentrations within the buoyant plume and assess the magnitude and persistence of dissolved hydrothermal Fe in basin scale deep waters and its impact on the Fe inventory of the deep ocean. We further explore general Fe solubility, biogeochemical reaction partners (dissolved organic matter (DOM) and nanoparticles), and biological activities (including exometabolites and Fe-cycling microbes) as potential factors that could influence the long-range transport of Fe from hydrothermal vents.

Irons hydrothermal journey

The early hydrothermal journey

Focused (near-endmember) hydrothermal fluids. While the significance of hydrothermal Fe fluxes to the deep ocean has been recognized, the geochemical controls that regulate Fe solubility at the vent source remain unresolved. Our analysis establishes these controls by correlating Fe concentrations with pH, temperature, spreading rate, and H_2S in vent fluids, thereby providing a quantitative foundation for assessing Fe stability and its subsequent transport in hydrothermal plumes. The composition of focused hydrothermal fluids, including concentration and speciation of Fe is generally considered to depend on a number of critical parameters[2]. We evaluate these critical parameters by analyzing MARHYS database Version 3.0. As we are interested in the behavior of hydrothermal Fe during its journey through the water column, we filtered the database to exclude calculated endmember compositions where all chemical species are back-calculated to a theoretical zero magnesium endmember. Global sampling of hydrothermal vent fluids has demonstrated that unmixed hydrothermal endmember fluids barely reach the seafloor surface and that high-temperature focused vent fluid samples contain on average ~5 mmol kg^{-1} of Mg, suggesting that these fluids often already contain ~10% of seawater. It is still questionable if this Mg is related to seawater entrainment during the sampling procedure, or if focused fluids typically entrain a certain amount of seawater in the subsurface just prior to being emitted. Chemical analyses of hydrothermal solutions furthermore suggest that vent fluids are typically either emitted slightly diluted as described above or highly diluted with Mg concentrations «45 mmol kg^{-1} and over 85% of seawater entrained[54]. As the available data of barely diluted vent fluids is more comprehensive and dilution trends would obscure controls on hydrothermal Fe, we restricted our analysis to the former group and excluded vent fluids with Mg concentrations >10 mmol kg^{-1} (the full dataset used for our analyses is given in Supplementary Table 1). The concentration and behavior of Fe are primarily controlled by the composition of host rocks and pressure and temperature conditions under which fluid–rock reactions occur in the hydrothermal reaction zone (Fig. 2a). These factors, in turn, influence pH (Fig. 2b), chlorinity (Fig. 2c), and sulfide concentration (Fig. 2d), which together assert control over Fe concentration and speciation. In mid-ocean ridge (MOR) basalt-hosted hydrothermal circulation systems, an inverse relationship between reaction zone depths (and corresponding temperatures and pressures) and spreading rate has been shown with tendency to shallower reaction zones at faster spreading ridges[56]. Concurrently, the reaction zone depths influence the mode of phase separation and determine the predominant occurrence of vapor- or brine-type hydrothermal fluids[57]. Phase separation processes have been shown to influence Fe and H_2S concentrations in hydrothermal fluids[58]. While Fe preferentially partitions into brines, the dominant sulfur species at hydrothermal temperatures (H_2S or HS^-) preferentially partitions into vapors. This behavior results in a correlation between chlorinity and the Fe/H_2S ratio for near-endmember hydrothermal fluids (Fig. 2e).

Among temperature, pH, and chlorinity, another strong control on vent fluid chemistry is caused by host rock composition, which is controlled by geodynamic processes underlying the hydrothermalism (i.e., tectonic activity along MOR, subduction of tectonic plates to form volcanic arcs or back-arc spreading, or formation of hot spot related intra-plate volcanoes). Hence, we sub-grouped the vent fluids according to the host-rock types given in the database (Supplementary Table 1). Because of over- or under-sampling at individual vent fields, the number of database entries for these vent fluid groups may not accurately represent their global occurrence, but they can provide a first-order approximation of their overall significance. Roughly half of the sampled hydrothermal fluids circulate through basaltic substrate at MORs (Fig. 3 and Supplementary Table 1). In fact, hydrothermal circulation is not limited to MORB-substrate, but according to the global fluid sampling as of today, the other half pertains different host-rocks (Supplementary Table 1); this other half occurs to roughly equal extents in ultramafic rocks (e.g., Northern Mid-Atlantic Ridge (MAR), Mid-Cayman Rise, etc.), as well as in sediments (e.g., Gulf of California, Gorda Ridge, Explorer Ridge, etc.), and in mafic (basalt), intermediate (basaltic andesite-andesite) and felsic (dacite-rhyolite) rocks in arc and back-arc environments (e.g., Tonga-Kermadec arc, Northeast Lau Spreading Center etc). Most hydrothermal vent fluid compositions are thought to be controlled by fluid–rock interaction with a single substrate, typically the host rock in which the vent orifices are located. However, some fluid compositions indicate interaction with multiple host rocks (e.g., ultramafic and basalt[59,60] or basalt and sediment[61,62]). Such mixed fluid-rock interactions are one possible explanation for the multimodal distribution of some species concentrations observed within vent fluid groups. Despite equal host-rock types, we discriminated between MORB-hosted fluids and mafic fluids at arcs and back-arcs as they discern by tendentially shallower water depths and subsurface reaction-zone depths in arcs and back-arcs. Fluid-rock interaction of basaltic rocks produces a wide range of compositions due to variable reaction zone depths and fluid-rock ratios. Since individual components of hydrothermal fluids are not normally distributed when binned to primary host rock types, we summarized properties of focused hydrothermal vent fluids via modal analysis, and we identified mode maxima within rock type and geological setting for the properties explored here (Fig. 4 and Supplementary Table 2). We did not mitigate against much sampled vent fields, since vent fluid composition can vary over time[63,64] as well as space and our aim was to give a broad overview of this variability within rock types. Peridotite produces vent fluids with highest Fe concentrations (highest mode maxima: 20.7 mmol kg^{-1}; Supplementary Table 2). It also stood out as a host-rock producing fluids with multimodal distributions of pH, temperature, H_2S, and Fe. The multi-modality likely reflects an influence of serpentinization, which typically occurs in peridotite hosted vents and results in chemical distinct fluids with high pH[65]. Distributions were unimodal in MORB and mode maxima for temperature, pH and Fe were similar to modes observed for peridotite (Fig. 4 and Supplementary Table 2). Nevertheless, the marked decrease in H_2S concentrations in peridotite-hosted vent fluids meant that Fe/H_2S ratios in MORB were lower (mode maxima: 397 mmol mol^{-1}) than the main Fe/H_2S mode observed for peridotite (mode maxima: 5122 mmol mol^{-1}). A bimodal distribution was also identified for Fe in vent fluids circulating through felsic substrate with mode maxima similar to the lower mode maxima of fluids in peridotitic substrate (Supplementary Table 2). Vent sites in sedimentary host rocks appear to have the lowest Fe concentrations.

Fe concentrations of up to 24.1 mmol kg^{-1} [66] have been observed at Rainbow in the northern MAR. These Fe concentrations are associated with sulfide concentrations of less than 3 mmol kg^{-1} in fluids with high chlorine concentrations of up to 773 mmol kg^{-1}. Basalt-hosted vent sites show high sulfide concentrations of up to 39.4 mmol kg^{-1} (as total H_2S) that are associated to Fe concentrations of only 1.3 mmol kg^{-1} as observed in chlorine-poor fluids (124 mmol kg^{-1} of Cl) at the East Pacific Rise (EPR) 9°N[67]. These fluids have been extrapolated to an H_2S concentration

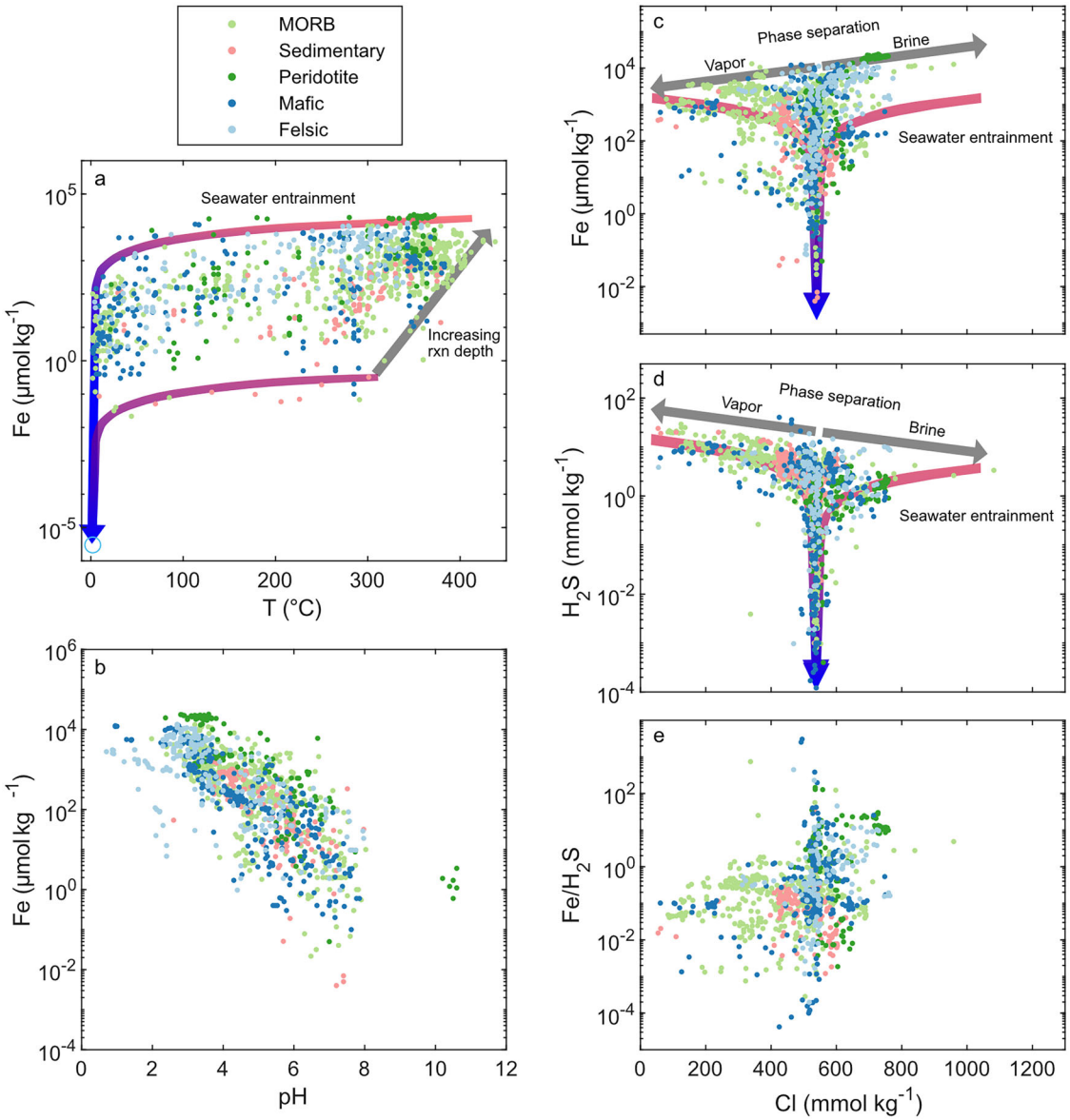

Fig. 2 | Controls on Fe and H2S concentrations in hydrothermal vent fluid samples as seen in MARHYS database Version 3.0. a Fe concentration vs temperature. The gray arrow qualitatively denotes increasing Fe concentrations with increasing reaction zone temperatures and depths. The curved arrows denote seawater dilution paths with conservative behavior of Fe for I) a 350 °C hot hydrothermal endmember fluid with a concentration of 0.5 mmol/kg Fe and II) a 450 °C endmember fluid with 50 mmol/kg of Fe. **b** Fe concentration vs pH value. Here, due to highly non-conservative behavior of pH during seawater mixing no dilution paths are drawn. **c** Fe vs chlorinity. Gray arrows qualitatively denote phase separation trends with a correlation of Fe and Cl (see Supplementary Fig. 1a, b). Colored and curved arrows denote an exemplary seawater dilution trend with conservative behavior of Cl and Fe. **d** Sulfide vs chlorinity with anticorrelation of H_2S and Cl (see Supplementary Fig. 1c, d). Arrows are as in (**c**). **e** Fe/sulfide ratios plotted against chlorinity. Note: that "mafic" (basalt-basaltic andesite) and "felsic" (andesite-rhyolite) vent fluids represent hydrothermal fluids in back-arc basins and volcanic arcs. MORB mid-ocean ridge basalt.

of 111 mmol kg^{-1} with an Fe concentration increased to less than 1 mmol kg^{-1} [64,68,69] in a nearly chlorine-free hydrothermal endmember (45 mmol kg^{-1} of Cl). These extreme examples show the fundamental control of phase separation processes, among phase relations between hydrothermal fluids and various rock types, on the delivery of Fe from hydrothermal vents into the ocean. Overall, vent fluid data suggest a regional clustering of Fe delivery to the oceans, with higher Fe inputs from peridotite-hosted vent sites into deep ocean water masses and an extraordinary role of felsic-hosted vent sites that release Fe in much shallower water depths from arc hydrothermal systems (e.g., ref. 70). In contrast sediment-related hydrothermal vents play only a subordinate role in delivering Fe and other transition metals into the ocean.

The DOM pool is critically important for Fe biogeochemistry in hydrothermal systems[71,72]. The molecular composition of DOM from hot fluids has been found to differ substantially from that of background seawater[73,74] with the recalcitrant DOM pool that makes up a large portion of seawater dissolved organic carbon (DOC) undergoing thermal degradation in hot fluids[75]. Enhanced DOC concentrations observed in hydrothermal fluids (e.g., ca. 600 μmol L^{-1}; MARHYS 3.0) are thought to arise as a result of thermally driven abiotic reaction DOCs between H_2, CO_2, CH_4, NH_3, and H_2S with resultant production of small molecules such as formate and methanethiol[76–79]. Production of small molecules is also influenced by thermal breakdown of the recalcitrant DOM present in the entrained seawater and entrainment of seawater that has been in contact with any surrounding biomass[76,78]. Nevertheless, the extent to which these types of compounds can influence the long-term stabilization of dissolved Fe in seawater is poorly understood. Where hot vent fluids lack elevated supplies of reducing volatiles, DOC

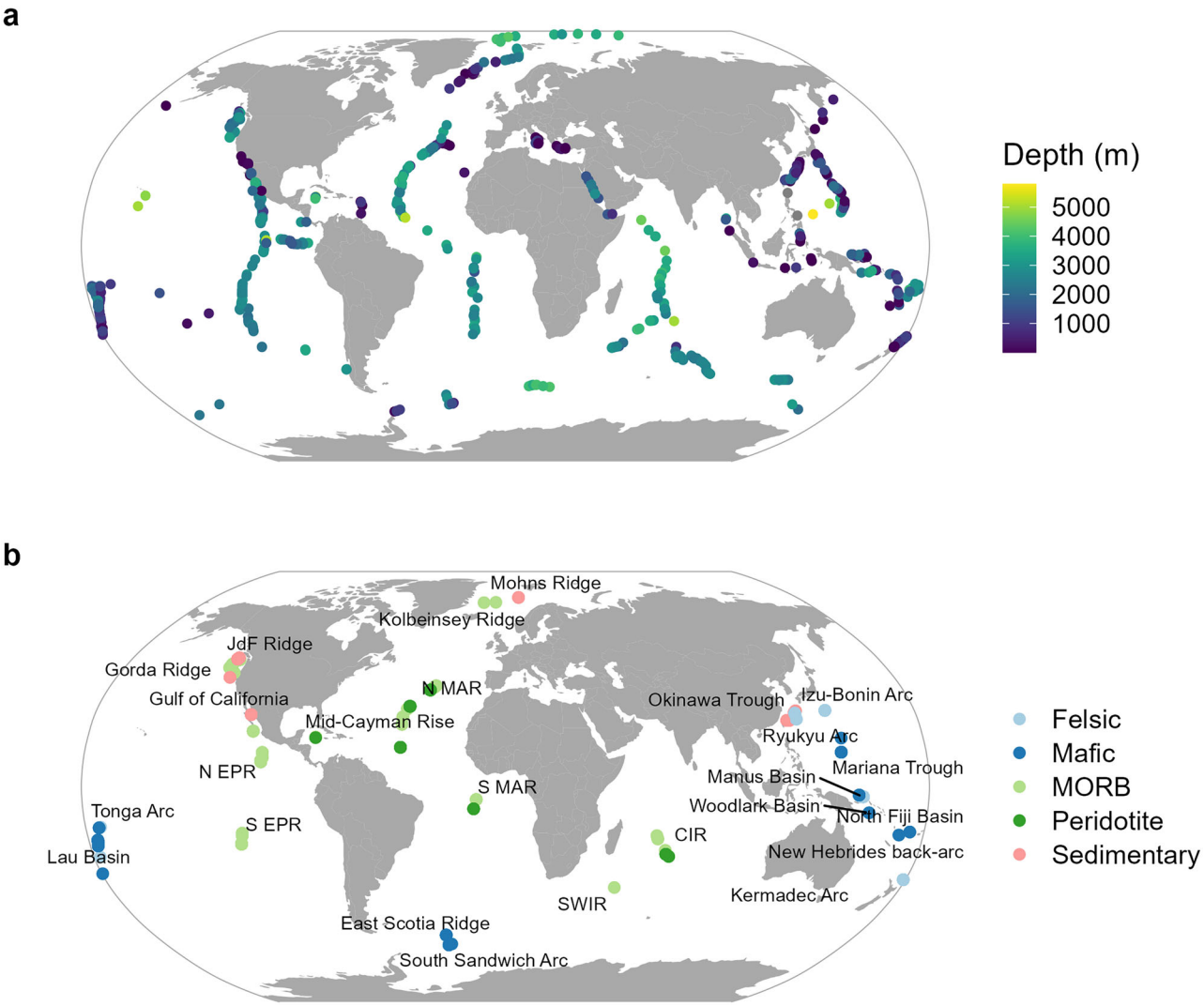

Fig. 3 | Distribution of vent sites recorded in the Inter Ridge database. a Depth and position of each vent site. **b** Vent sites with associated vent fluid characteristics recorded in MARHYS database and summarized in this study. Color shows primary rock type recorded for each site. MORB - mid-ocean ridge basalt.

concentrations are typically depleted to concentrations of the order of 10–20 μmol L^{-1} [80].

Diffuse fluids. Diffuse venting occurs either close to focused hot vents, when high-temperature fluids mix with cold seawater in the subseafloor[81,82] or by limited water-rock reactions and conductive heating during shallow fluid circulation[83,84], which can also result in off-axis diffuse fluids away from the ridge axis[85]. Furthermore, areas on slow-spreading ridges with thick oceanic crust like at 9°S on the Mid-Atlantic Ridge, where the Lilliput hydrothermal vent field was discovered[86] appear to show more abundant diffuse venting as compared to focused hot venting. Diffuse venting is usually recognized visually as shimmering water or by the occurrence of microbial mats and specific vent biota. Due to the lower temperature (from <0.2 °C to ~100 °C[87]), the dissolved metal load is much lower compared to that of hot vents. However, Bemis et al.[87] also compared the focused and diffuse mass flow rates from EPR 9°50′N, and obtained a total Fe input of $FFe_{focused}$ = 35 mmol s^{-1} from high-temperature vents and $FFe_{diffuse}$ = 132 mmol s^{-1} from diffuse-flow vents, respectively. Thus, the flow rate of Fe from diffuse flow sites at EPR 9°50′ N is nearly four times that from high-temperature vents. In a modeling study, German et al.[88] indicated that the majority of Fe supplied to hydrothermal plumes may originate from diffuse outflows. Their model predicted that dissolved Fe concentrations in diffuse hydrothermal flow worldwide, are on the order of 10–100 μmol kg^{-1}, implying that diffuse-flow hydrothermal fluxes likely dominate the supply of dissolved Fe from hydrothermal systems to the deep ocean. In some cases, measured concentrations exceed these modeled values by orders of magnitude. For example, at the Lilliput vent field, dissolved Fe concentrations of up to 43 mmol kg^{-1} were measured in low-temperature (~10 °C), mildly acidic (pH ~6) fluids, surrounded by extensive Fe oxyhydroxide encrustations[86], suggesting that this vent field is an intense Fe source to the deep ocean.

Collectively, such findings suggest that the extent of fluid flow exceeds that of focused flow in terms of both fluid mass flux and energy transport, making diffuse hydrothermal discharge a more important and at the same time overlooked source of Fe to the ocean[88,89].

The diffuse flow and the surrounding seawater have been considered to be a source of DOM to the system, which could have a significant impact on the solubility and transport of Fe from diffuse vents. Diffuse flow systems can alter the composition of DOM and be a source of more labile organic carbon[90–94]. Thus, diffuse venting could be an important mechanism for stabilizing dissolved Fe through the formation of stable organic Fe complexes.

A recent analysis of MARHYS database confirms this important role for diffuse venting to the global hydrothermal Fe budget[95]. If 90% of the globally advected heat is removed via diffuse flow instead of focused hydrothermal venting, the hydrothermal Fe input to the ocean is diminished

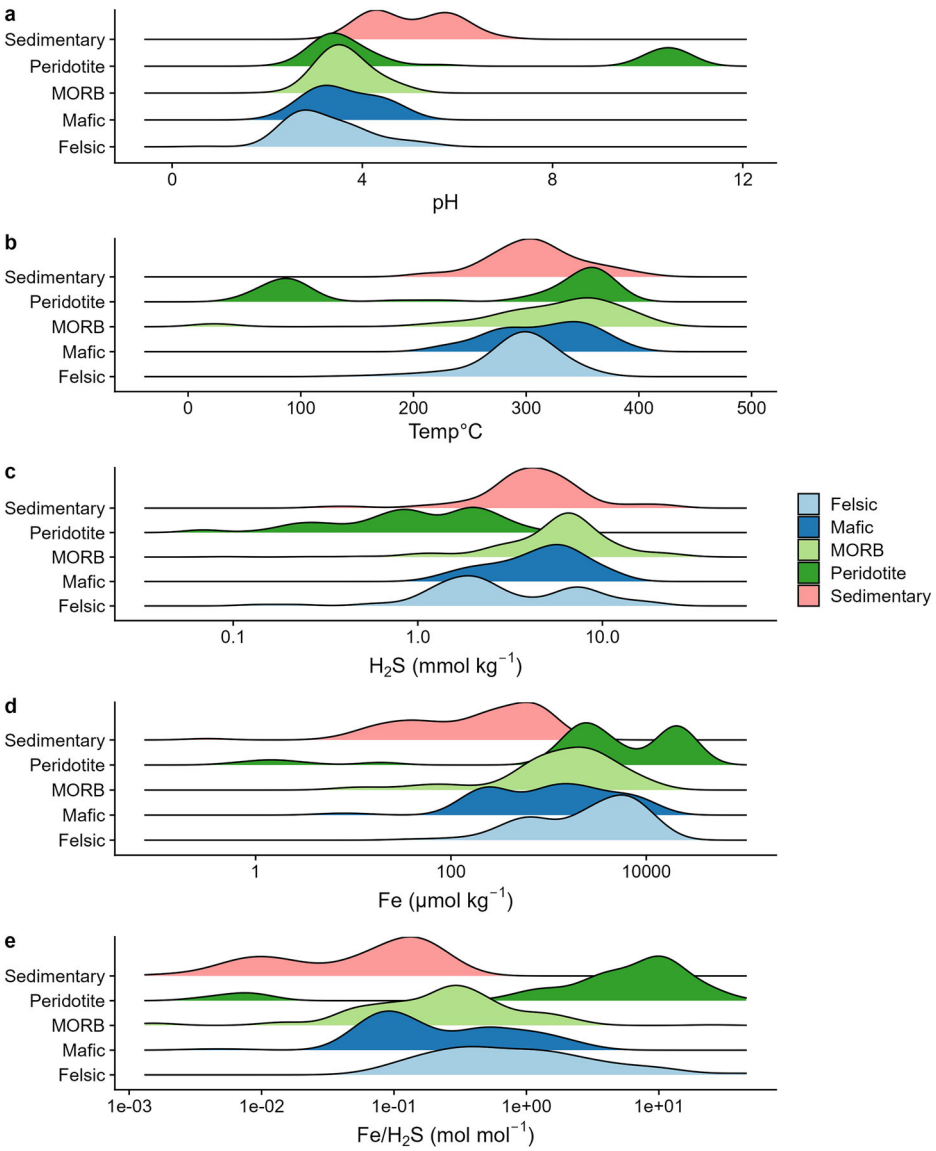

Fig. 4 | Distributions of key physical and chemical properties within focused hydrothermal fluids (Mg <10 mmol kg^{-1}) of different primary rock types. a pH, (**b**) Temperature, (**c**) H_2S, (**d**) Fe and **e** Fe/H_2S. Properties corresponding to the range and maximum density for each identified mode are provided in Supplementary Table 1. MORB - mid-ocean ridge basalt.

by ~75% due to subsurface mineral precipitation. The corresponding focused and diffuse Fe fluxes at basalt-hosted mid-ocean ridges were calculated as 7.7 Gmol yr^{-1} (diffuse) and 5.2 Gmol yr^{-1} (focused). This global evaluation confirms the prior mentioned studies and assigns diffuse venting a dominating role in contributing Fe to the oceans.

Despite the confirmed important role of diffuse venting for hydrothermal Fe fluxes into the deep ocean, the following chapters will focus on hot venting processes as these have been studied in much more detail, while compositions and fluxes of diffuse vents still warrant more detailed studies in the future.

Vent-orifice–proximal hydrothermal processes

Abiotic processes. In the high-temperature realm the geochemistry of Fe is abiotically controlled by its oxidation state (Fe(II)/Fe(III)) and by the relative affinities of the two oxidation states for complexation with sulfur and oxygen containing moieties. Fe(II) has a higher affinity for moieties containing reduced sulfur (e.g., sulfides), while Fe(III) has a higher affinity for those containing oxygen (e.g., hydroxide ions). Both Fe(II) sulfides and Fe(III) hydroxides are rather insoluble in water[96,97] (see also Box 1), and both phases have been observed in vent particles (e.g., refs. 71,98) although the solubility of both species increases with decreasing pH and temperature. To provide some context for the calculated solubilities shown in Box 1, the maximum concentration of total sulfide in focused fluids recorded to date is 29 mmol kg^{-1} on the EPR[99] (Fig. 4) and was associated with Fe concentrations of 1.3 mmol kg^{-1}, pH 3 and a temperature of 380 °C, while maximum Fe concentrations of 24 mmol kg^{-1} are recorded in focused fluids at the Rainbow site in the Mid Atlantic Ridge, with a total sulfide concentration of 3 mmol kg^{-1}, a pH of 3.6 and a temperature of 350 °C[66,76]. At 25 °C, pH 3 and total sulfide concentrations of ca. 100 mmol L^{-1}, the solubility of FeS (defined by 0.2 µm filtration) is of the order of 30–50 mmol L^{-1}[97]. The solubility of Fe(III) hydroxide at pH 3 (in the absence of sulfide and defined by filtration cut off of 0.02 µm) is ca. 1 mmol L^{-1}[196]. Although the formation of $Fe(OH)_3$(s) and FeS(s) is promoted by higher temperatures (Box 1), there is currently insufficient data to know if the relationships observed at ambient seawater temperatures persist into temperature experienced by hydrothermal fluids. Both $Fe(OH)_3$(s) and FeS(s) form colloids (0.02–0.2 µm) and FeS and $Fe(OH)_3$ colloids can be determined in what is typically termed the dissolved phase.

Fe:H_2S ratios have been used to identify sites where Fe loss by sulfide precipitation in the plume is important[46,47,100]. Vents with low Fe:H_2S ratios (typically in the range 0.3–1.0), like TAG, Snakepit, and EPR and are considered to be sites where sulfide precipitation is important[101,102], whilst at vents with high Fe:H_2S ratios (>100), such as many along the Mid-Atlantic Ridge, negligible precipitation of Fe sulfides has been observed[103,104]. Figure 5 shows the global distribution of the median Fe:H_2S ratios determined for vent sites in focused fluids where Fe:H_2S ratios could be calculated from the

Box 1 | Solubility (for calculations, please refer to Supplementary Note 1)

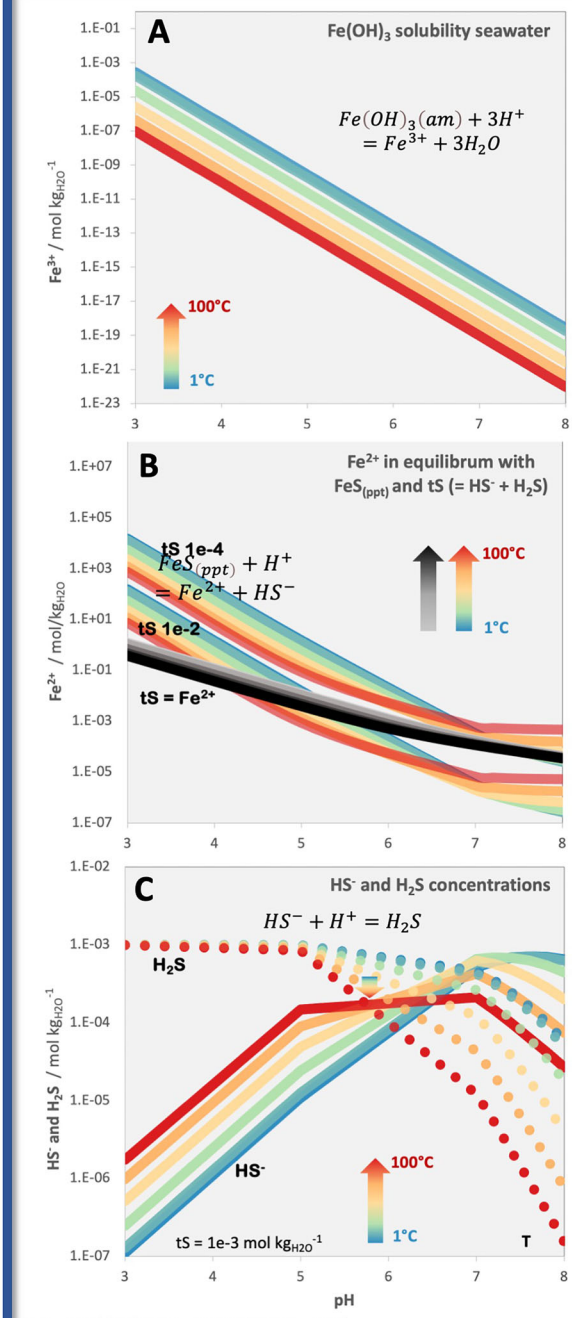

Inorganic Fe^{3+} solubility in seawater with respect to $Fe(OH)_3$ **(A)** is strongly pH dependent, where Fe^{3+} concentrations decrease by approximately three orders of magnitude over one unit increase in pH (= $-\log_{10}[H^+]$).

$FeS_{(ppt)}$ solubility **(B)** in seawater (grey scale) is also strongly pH dependent albeit to a lesser extent. Here dissolved sulfide (tS) concentrations and their speciation (tS = HS^- + H_2S) add an additional control. In seawater (no initial tS present) $FeS_{(ppt)}$ solubility is characterized by equal (molar) concentrations of tS and Fe^{2+} (grey scale plots).

In equilibrium, the product of HS^- and Fe^{2+} has to remain constant so that in high sulfide fluids Fe^{2+} is capped at lower concentrations and vice versa. Keeping in mind that only HS^- (not H_2S) is a reaction partner for $FeS_{(ppt)}$ solubility, the speciation of tS and its pH dependence **(C)** also exerts a crucial role in Fe^{2+} regulation. At acidic pH, tS is mainly present as H_2S, thus allowing high Fe^{2+} concentrations at a constant $[Fe^{2+}][HS^-]$ equilibrium product. Between pH 6-7, HS^- becomes the dominant species capping Fe^{2+} at significantly lower concentrations.

The temperature influence is added for comparison. Both $Fe(OH)_3$ and $FeS_{(ppt)}$ solubility decreases with increasing temperature. This effect is reversed for $FeS_{(ppt)}$ at alkaline pH due to the strong temperature influence on tS speciation **(C)**. Note, that while the chemical data is reliably available at 25°, towards 100° the strong temperature influence might be a side effect of an inaccurate temperature correction of the chemical input data (see supplementary material for more details on the equilibrium calculations)

MARHYS database, fourteen sites have Fe:H_2S ratios <0.03, whilst 23 have Fe:H_2S ratios >3.

To further improve understanding of factors influencing Fe during initial mixing of vent fluids with seawater we examined correlations between pH, temperature, spreading rate, H_2S and Fe (Fig. 6 and Table 1) in our focused hydrothermal fluid dataset. Correlation coefficients between $\log_{10}$(Fe) and pH were higher than those with $\log_{10}(H_2S)$, with pH clearly correlating most strongly with $\log_{10}$(Fe) concentrations (Fig. 2). This likely reflects the strong relationship between pH and the solubility of Fe minerals formed in the focused vent fluids (Table 1 and Box 1). Since pH itself is

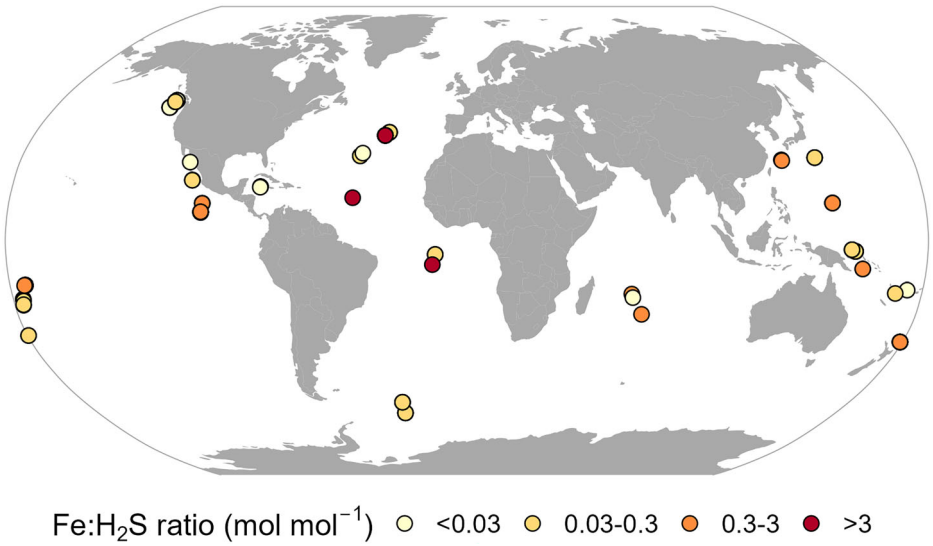

Fig. 5 | Median Fe:H2S ratios (mol mol^{-1}) observed in focused hydrothermal fluids at 143 sites where both H2S and Fe were present in the database. Median values were binned based on the density distributions observed in Fig. 4.

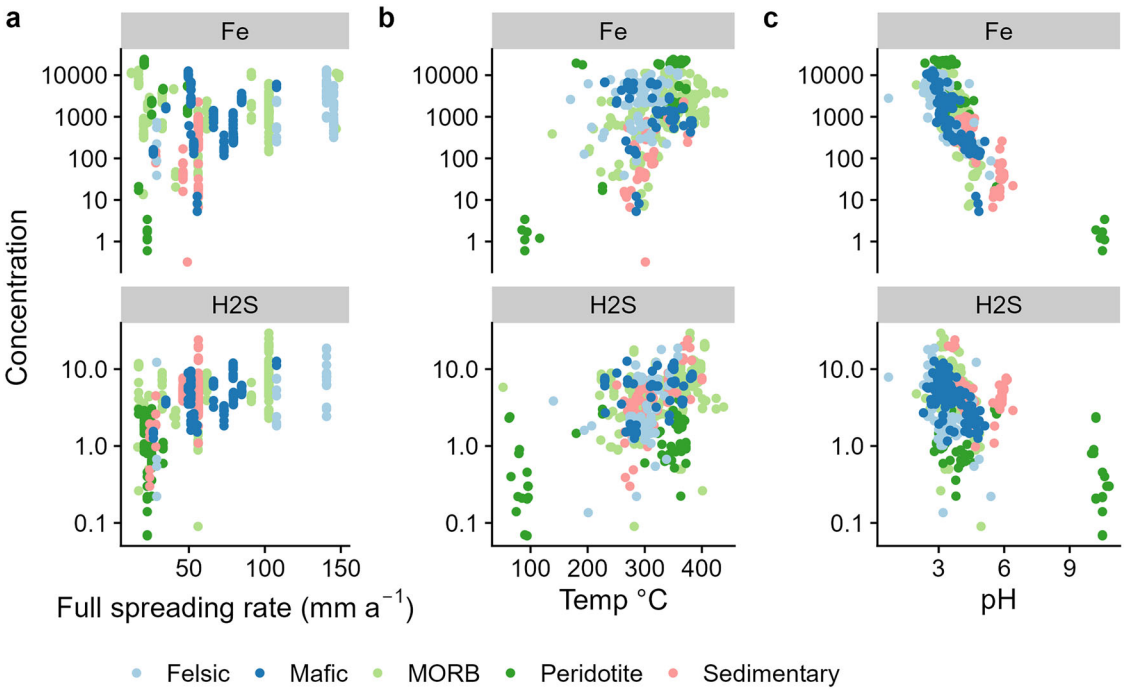

Fig. 6 | Relationship between key vent properties and Fe (μmol kg^{-1}) and total H_2S (mmol kg^{-1}) contents. a Spreading rate, (**b**) Temperature and **c** pH of focused hydrothermal fluids. Four observations where H_2S <0.1 μmol kg^{-1} were not plotted to aid visualization of the H_2S data.

strongly influenced by the temperature of rock water interactions, fluid temperature and pH exhibited a high correlation coefficient (Table 1), and pH also correlated with spreading rate, nevertheless, it was notable that Fe did not correlate with spreading rate ($p = 0.04$, $n = 168$).

Microbial processes. Microbes living in hydrothermal vent environments are metabolically diverse and mediate a variety of biogeochemical processes that involve and connect the carbon, sulfur, hydrogen, nitrogen, and metal cycles[105]. Here, the microbially mediated redox transition between Fe(II) and Fe(III) is one of the most critical processes from the perspective of iron speciation and bioavailability in hydrothermal systems, as this transformation strongly governs nanoparticulate iron formation, solubility, and ultimately the transport of iron into the ocean. At the same time, this transition is one of the biochemically least understood redox reactions, as currently neither the key enzymes involved, nor the detailed physiologies and dependencies are known[106]. Indeed, most of our knowledge on Fe-metabolizing microbes in marine environments is based on only a few cultured representatives[105,107].

Dissimilatory Fe-reducing microorganisms (FRM) utilize extracellular Fe(III) as a terminal electron acceptor and reduce it to Fe(II)[108] (Fig. 7). This form of energy metabolism is widespread across diverse bacterial and archaeal lineages and is active under a variety of environmental conditions[106]. The steep thermal and also chemical gradients along the fluid pathways at hydrothermal vents provide numerous niches for FRM to colonize surfaces and pores of mineral deposits[109]. Yet only a few isolates, mainly from the bacterial phyla *Thermotogota*, *Deferribacterota*, *Desulfobacterota*, *Thermodesulfobacteriota*, *Bacillota A*, *Deferrisomatota* and *Pseudomonadota* as well as the genus *Thermococcus (Archaea)* have been obtained in pure culture[110–120]. Fe and S rich minerals not only provide the energy sources for FRM, they also protect these microbes from harsh

Table 1 | Correlation coefficients calculated between spreading rate, temperature, pH, log_{10}(Fe) and log_{10}(H_2S) in focused hydrothermal fluids (Mg <10 mmol kg^{-1})

	Spreading rate	Temperature	pH	$Log_{10}(H_2S)$	Log10(NH_3)
$Log_{10}Fe$		0.46 (0.39, 0.53) $n = 528$	−0.79 (−0.82, −0.75) $n = 577$	0.20 (0.10, 0.27) $n = 496$	−0.65 (−0.73, −0.56) $n = 179$
$Log_{10}(H_2S)$	0.47 (0.28, 0.63) $n = 80$	0.49 (0.42, 0.56) $n = 494$	−0.51 (−0.57, −0.45) $n = 541$		
pH	−0.42 (−0.52, −0.3) $n = 206$	−0.74 (−0.707, −0.70) $n = 601$			

Mean log_{10} concentrations were used for correlations with spreading rate. Only correlations where $p < 0.01$ are shown. Values in brackets show lower and upper confidence intervals.

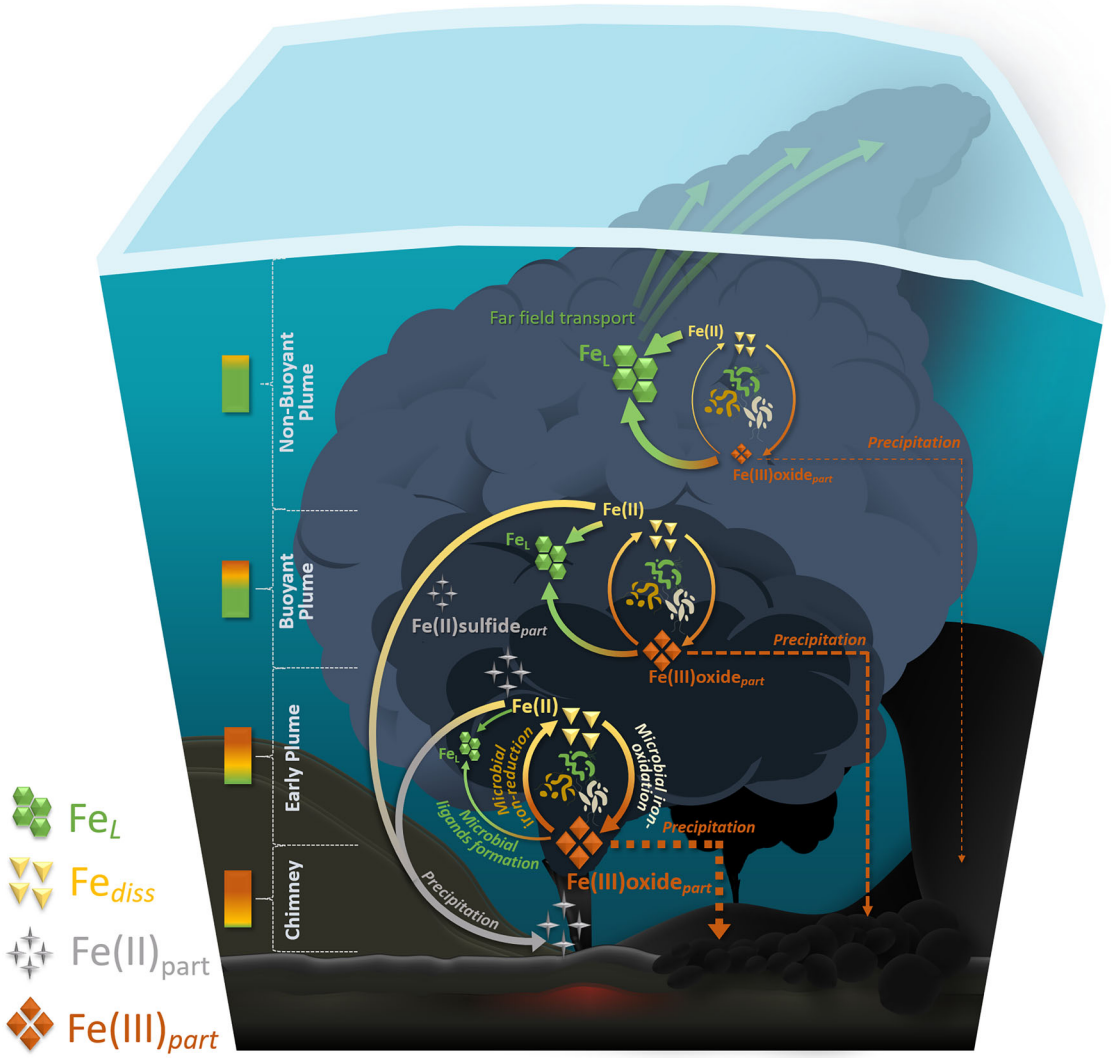

Fig. 7 | Schematic overview of a deep-sea hydrothermal vent plume illustrating microbially mediated Fe redox reactions in the early, buoyant, and non-buoyant plume. Symbol sizes for various Fe species reflect their relative abundance, while arrow thickness represents the frequency of Fe-related processes. Larger symbols and thicker arrows correspond to higher relative abundances or frequencies, respectively.

environmental conditions such as thermal fluctuations[121], which may enable them to withstand short term temperature increases. FRM though can thrive under extreme thermal conditions and one hyperthermophilic isolate has even been shown to survive at temperatures near the upper limits of microbial life[122,123].

Fe oxidizing microbes (FOM) convert the soluble Fe(II) into the insoluble Fe(III) form, which often precipitates as Fe(III) oxyhydroxides (Fig. 7). FOM are widespread in diffuse-flow hydrothermal vent areas across the world's ocean[107], with the majority of species belonging primarily to the phylum *Pseudomonadota* (synonym *Proteobacteria*[124]), including representatives of *Alphaproteobacteria*[125], *Betaproteobacteria*[126], *Gammaproteobacteria*[127,128] and *Zetaproteobacteria*[129,130]. *Zetaproteobacteria* were discovered only 15 years ago at Fe-rich low temperature hydrothermal vents of the Kama'ehuakanaloa Seamount (formerly Loihi) and build a phylogenetically new class of Fe oxidizers[131–133]. They form tangled stalks of Fe(III) precipitates that consist of polysaccharides and adsorbed organic exudates providing a reservoir of organic carbon for heterotrophic and fermenting microbes[129]. Significant correlations between the abundance of specific zetaproteobacterial OTUs and the occurrence of distinct Fe oxide morphologies in Fe-rich microbial mats of the Lucky Strike hydrothermal field suggest that the formation of Fe-oxide morphologies may be both taxonomically and ecologically

determined[130]. Strains of the genus *Zetaproteobacteria* namely *Mariprofundus* have been discovered repeatedly in low temperature hydrothermal habitats, where they are expected to play a major role in Fe, carbon and nutrient cycling[134–137] (and references therein). Within the *Gammaproteobacteria* members of the genus *Marinobacter* were reported to have nitrite-dependent Fe-oxidizing capabilities[125,127] (and references therein). Recent work has more so shown that within the gammaproteobacterial *Hydrogenovibrio / Thiomicrospira* clade at least one strain, that was isolated from the Indian Ridge (IR), has the ability to oxidize Fe, alongside with hydrogen and reduced sulfur compounds for generating energy and subsequently fixing CO_2[128]. This is the first documentation of a metabolic flexibility in such a genus suggestive of its adaptation to dynamic conditions prevailing in hydrothermal vent systems. Laboratory experiments with microbes from fluids of the Fe-rich Brothers volcano (Kermadec) showed that members of the *Hydrogenovibrio/Thiomicrospira* genera were significantly enriched if Fe or hydrogen was added and most biomass synthesized from CO_2 fixation when Fe was supplied[138]. To date only one strain of the *Hydrogenovibrio/Thiomicrospira* clade has been demonstrated to be involved in Fe cycling and this bacterium was not associated with hydrothermal environments[139,140]. Since they are ubiquitously abundant at vent sites, their role for Fe acquisition and cycling needs to be further studied. In contrast, in the Fe-poor Haungaroa fluids no enrichment of putative Fe oxidizers was noted, albeit the highest CO_2 fixation was measured after Fe additions to the experiments[138]. Nevertheless, in Fe-amended sediment slurries from Haungaroa, where Fe_2O_3 total was 6.3 wt%, *Sulfurovum* became enriched and some of the highest CO_2 fixation rates were measured after Fe addition[138]. Despite Fe-uptake genes are encoded on the genome of *Sulfurovum*[141], the actual role of *Sulfurovum* in Fe cycling remains unknown.

The later hydrothermal journey: hydrothermal plumes

The buoyant hydrothermal plume. The buoyant hydrothermal plume is a rising column of fluid expelled from a hydrothermal vent which continuously mixes with the surrounding seawater. It rises in the water column due to fundamental principles of fluid dynamics and thermodynamics: as seawater is heated, it becomes more buoyant compared to the surrounding colder seawater which creates a column of hot, metal-enriched fluid that can reach several hundred meters to kilometers in height[142]. Subsequent mixing and cooling lead at some point to the creation of a neutrally buoyant plume.

In early studies from Rudnicki and Elderfield[41], it was stated that about half of the Fe in the high temperature vent fluid is removed as sulfides within a few seconds of venting and that the remainder is removed by Fe^{2+} oxidation (Box 1). The turbulent entrainment and mixing of ocean water into early plumes enhance precipitation of dissolved Fe[143], but part of the hydrothermal Fe stays within the plume and can still be measured several hundred[144] to thousands of kilometers from the vent[42].

Initially, metal sulfides form, and later, as the rising plume becomes more oxic, Fe oxides precipitate. This is partly a consequence of the temperature change, which affects the solubility of many minerals[145], and the alteration of the pH and Eh of the solution due to mixing. The higher pH and lower temperature induces the precipitation of metal sulfide minerals[146]. Much of the trace element chemical reactivity observed in plumes is also attributed to the precipitation and surface reactivity of Fe (oxy)hydroxide minerals in the buoyant plume[143], which are also held responsible for scavenging of other elements from the surrounding seawater into the plume (e.g., vanadium, thorium, and neodynium[44]).

To explain transport of dFe in the rising plume, mechanism(s) must stabilize it against precipitation, aggregation, and scavenging losses, and many recent studies have investigated these processes. Waeles et al.[147] conducted in situ filtration experiments on early plume stages from diverse vent systems along the Mid-Atlantic Ridge (MAR) and found that over 90% of Fe remained in the dissolved fraction. This observation is consistent with basalt-hosted systems characterized by low Fe:H_2S ratios, where sulfide precipitation is suppressed, and pyrite formation is kinetically limited. Within our MARHYS framework, these findings align with other data (e.g., refs. 100,148), which show that Fe remains largely nanoparticulate or colloidal in environments with specific lithological characteristics—namely basaltic compositions with reduced sulfide enrichment.

Especially black smoker systems are discussed as important channels for Fe transport and dispersion into the deep sea by pushing nanoparticle-sized Fe-rich sulfides and oxyhydroxides[149] several tens to hundreds of meters above the sea floor[150], where they persist and dissolve to varying degrees. Pyrite nanoparticles have been found to be produced within the first meters of the buoyant plume[46,47,100,151]. They can comprise up to 60% of the filtered Fe (≤0.2 µm) one meter from the vent orifice and their persistence is an important mechanism for near-vent Fe stabilization and element transport[151]. Yücel et al.[46] report from the EPR and the Eastern Lau Spreading Center that pyrite nanoparticles account for up to 10% of the filterable Fe (less than 200 nm in size) in these waters. Nano-scale particles settle from the water column at rates of only a meter or two per year, giving them the opportunity to travel further away from the vent[46]. Nanoparticulate metal sulfides do not oxidize rapidly under standard conditions[152,153], and at typical ocean bottom water temperatures of 2–4 °C oxidative processes would be approximately four times slower[154].

Findlay[154] investigated partitioning in the first 1.5 m of three vent fields along the Mid-Atlantic Ridge and found Fe primarily in the <0.2 µm (filtered) portion. Significant concentrations of HNO_3^-extractable metals were found in the <0.2 µm fraction at all three vent sites, indicating that they likely exist in a recalcitrant nanoparticulate phase such as pyrite or chalcopyrite, in line with Yücel et al.[46]. In contrast, a rapid decrease in dFe concentrations has been described in surface and near medium-water depth hydrothermal sources within the Tonga-Kermadec arc, which was explained by a shorter residence time of surface water masses combined with several biogeochemical processes at play (dilution, precipitation, scavenging, biological uptake, and photoreduction)[155].

The presence of Fe-binding ligands can shift the balance between precipitation and dissolution, effectively increasing the solubility of Fe in hydrothermal plumes[49,156]. Such ligands include siderophores and other biologically derived molecules that bind Fe with high affinity, preventing or delaying its transformation into insoluble phases[50,157]. A study by Kleint et al.[157] found iron binding ligand concentrations up to micromolar and in excess compared to labile Fe concentrations for all samples in the buoyant plume of high temperature Nifonea vent field in the Coriolis Trough (SW Pacific); only a small fraction of up to 11.8% was found to be chemically labile. Wang et al.[158] measured speciation and Fe-binding ligands in the Mariana back-arc hydrothermal plume. The plume samples over the low-temperature Burke had the highest dissolved Fe/total Fe (dFe/TFe) of 82.2 ± 8.8% and labile Fe/total Fe (FeLab/TFe) of 53.3 ± 9.2%, suggesting that most of the dFe may be present as weakly crystalline Fe-oxyhydroxides and organic Fe complexes.

Toner[71] described the preservation of Fe(II) by potentially microbially-produced carbon-rich matrices that prevent oxidation and/or precipitation as insoluble minerals. Microbial Fe transporters are highly expressed in the Guaymas Basin deep-sea hydrothermal plume, which suggest a "microbial Fe pump" as an important mode of converting hydrothermal Fe into bioavailable forms[159]. Bennett et al.[160] provided evidence for in situ microbial productivity by chemolithoautotrophs, including Fe-oxidizing microorganisms, within the Kama'ehuakanaloa hydrothermal plume, where the absence of hydrogen sulfide within the fluids and the presence of an oxygen minimum zone results in a prolonged presence of reduced Fe. Hyperthermophilic archaea rapidly respond to changes in metal concentrations; they appear to possess diverse mechanisms for metal detoxification, dissimilatory metal reduction, and metal assimilation[161]. Fullerton et al.[162] described dissolved Fe concentration as the strongest driver of community structure in the early plume. Several microbial taxa specifically tied to iron metabolism have also been identified in rising plumes. Members of the Campylobacterota (such as *Sulfurimonas*) and Gammaproteobacteria (SUP05)

dominate these communities[163–166]. Notably, while *Sulfurimonas* have been demonstrated to be involved in manganese reduction[167], (links to Fe cycling only suggested), SUP05 appears to be directly involved in Fe cycling[168].

In summary, biogeochemical processes in the buoyant plume are fundamental in connecting the Fe flux from the source, i.e., the hot focused hydrothermal vent fluid to the near- and far-field ocean. The balance between continued precipitation of sulfide and oxide phases, promoting early loss of hydrothermal Fe, and the formation of nanoparticulate Fe sulfides, oxyhydroxides, and organically complexed Fe, forming soluble and transportable Fe phases, ultimately controls which fraction of hydrothermal Fe can escape the near-field environment and become part of the general deep ocean Fe cycle.

The non-buoyant hydrothermal plume. The transition from buoyant to non-buoyant behavior in a hydrothermal plume is a complex process mainly driven by density and temperature differences between the rising plume and the surrounding waters and is ultimately determined by the rate of seawater entrainment[41]. This entrainment gradually cools and dilutes the plume, reducing its density contrast with ambient water until it becomes neutrally buoyant and stops rising. At that point, the plume transitions from a narrow rising column into a laterally spreading layer[169]. A series of laboratory experiments by Carazzo et al.[170] simulating hot particle-laden plumes show that they are capable of forming stable neutrally buoyant clouds.

Fe is present in the non-buoyant hydrothermal plume in a variety of forms (dissolved and particulate, associated with slowly sinking particles and stabilized by organic molecules); although >90% of particulate Fe (pFe) can get lost within the first 200 km off-source (depending on the fluid composition), whereas ^{3}He as a conservative component in hydrothermal plumes decreases by a factor of just two to three[42], dissolved Fe can be detected at distances up to several thousand kilometers from the source, greatly affecting global biogeochemical budgets (e.g., refs. 24,42,171). Hydrothermal activity may also represent a major source of dissolved Fe throughout the South Pacific deep basin today[172]. Considerable Fe transport could also be detected within the neutrally buoyant plume from the TAG vent site (Mid Atlantic Ridge), where dFe concentrations ranged from 51 ± 2 nmol kg^{-1} right above the vent site to 1.56 ± 0.02 nmol kg^{-1} at the most distal station[173].

The results of a coupled 5-box model that covers the density range of the non-buoyant plume over the first 30 km distance from the vent site and that describes aggregation, disaggregation, advection and sinking of dissolved (colloidal) and particulate iron and manganese, showed that aggregation processes controlled dFe concentrations closer to the vent, while disaggregation processes became more prevalent further away, leading to the formation of Fe aggregates of varying sizes[174]. Gartman and Findlay[43] challenged the traditional understanding of metal removal from the plume, by suggesting that oxidation of Fe and manganese does not consistently result in their removal and that different rates of oxidation of hydrothermal Fe have implications for the dispersion of the produced oxide phases[175]. Furthermore, stabilization of Fe as stable complexes and in the form of nanoparticles that physically behave like dissolved compounds contribute to the long-range transport of hydrothermal Fe. Besides inorganic complexation, metal chelating molecules (so called ligands, such as e.g., siderophores) are known to play a major role in stabilizing hydrothermally derived Fe in its dissolved form[38,49,157,158,176–178]. The synergy of organic complexation and nanoparticle transport is central to understanding how hydrothermal Fe transcends its site of origin, shaping large-scale marine biogeochemical cycles. While buoyant and non-buoyant plumes, as well as diffuse low-temperature venting, each present different pathways for Fe release, all can be profoundly influenced by the presence of ligands. This complex interplay assures that the legacy of hydrothermal Fe extends far beyond the confines of vent fields, underscoring the need to better quantify these processes in a rapidly changing ocean. When hydrothermal plumes reach the photic zone—which can occur, for example, in regions of intense upwelling—organically complexed Fe can fuel primary productivity, connecting deep hydrothermal processes to surface ocean ecosystems[44,179], whereas shallow hydrothermal systems may directly fuel photosynthesis (e.g., ref. 180).

Understanding the processes that control the exchange of Fe between the soluble (<0.02 µm), colloidal (0.02–0.2 µm) and particulate (>0.2 µm) size fractions is especially critical for establishing the impact of hydrothermal plumes on the inventory of Fe. Lough et al.[144] investigated the behavior of Fe species within the Beebe vent buoyant versus non-buoyant plume (Piccard vent field, Caribbean Sea). They showed that during ascent of the buoyant plume, a significant fraction of particulate Fe was lost due to settling and exchange with colloids, whereas in the non-buoyant plume pFe concentrations increased during dilution, and colloidal Fe concentrations decreased apparently due to colloidal aggregation. Findlay et al.[151] also found that nanoparticulate pyrite is not immediately removed from the plume. Hoffman et al.[181] further confirmed the presence of Fe-carbon composite particles in the non-buoyant plume, indicating the potential for Fe transport through strong biological modification. Transcriptomic analyses from the Guaymas Basin hydrothermal vents indicated that 70% of Fe-related bacterial transcripts are associated with siderophore acquisition, regulation, and biosynthesis[159]. Another study by Hoffman et al.[182] presents the first measurements of siderophore concentrations in hydrothermal vents along the Mid-Atlantic Ridge, showing that their presence and diversity are influenced by how close they are to the vents, indicating that biological processes play a key role in Fe chemistry in these systems.

Fe isotopes as tools for tracing the fate of hydrothermal Fe

Fe isotopes are a potential tool for tracing the biogeochemical redox cycle of Fe in the ocean[183]. Hydrothermal fluids show a range in Fe-isotopic composition that is shifted to low δ^{56}Fe values by −0.2 to −0.7‰ compared to igneous rocks[184–187]. Fe isotope compositions are transformed within a hydrothermal plume and may differ from that of the original vent fluids. Fe isotopes of the high-temperature fluid sources and the neutrally buoyant plume and underlying sediments from the Rainbow hydrothermal vent site are indistinguishable, while particles from the early buoyant plume show higher isotopic values due to fractionation during the oxidation process[103]. A study by Nasemann et al.[188] on dissolved Fe isotope data from two buoyant plumes and profiles traversing the non-buoyant plume above the Nifonea vent field in the Vanuatu back-arc found opposing controls from precipitation of Fe sulfides and Fe-oxyhydroxides that either enrich the heavy or the light isotopes within the residual dissolved Fe fraction, but also suggest significant influence from size partitioning of oxidized Fe following precipitation as well as potential effects from organic complexation. Especially under limited Fe oxidation and precipitation the role of Fe-sulfide precipitation during early plume rise determines the isotope signature of hydrothermal Fe exported to the open ocean. Sulfide-rich basalt-hosted hydrothermal systems and slow oxidation kinetics in the Pacific favor export of stabilized dissolved Fe with heavier δ^{56}Fe values than the true vent fluids. Bennett et al.[189] found that 25% of Fe precipitates as Fe-sulfides, leading to a specific isotope fractionation value in the plume. Another study coupling Fe ligands and isotopes in hydrothermal plumes over backarc volcanoes in the Northeast Lau Basin[183] found that δ^{56}Fe increased during plume dispersal and dilution. This trend was attributed to the preferential loss of particulate Fe-sulfides or Fe-oxyhydroxides, depending on H_2S concentrations and Fe/H_2S ratios. This shows that hydrothermal plumes can export dissolved Fe with a significantly heavier δ^{56}dFe than the original vent fluids. For the first time, a positive correlation was observed between δ^{56}dFe and the conditional stability constants of iron-ligand complexes (FeL), indicating that organic complexation may influence the Fe isotopic signature along the plume. The long-term influence of hydrothermal venting activity on Fe isotopic composition of the deep ocean is also evident in a ferromanganese crust from the hydrothermally

active Izu Bonin backarc, which recorded variable hydrothermal input over a period of about 10 million years, correlating with changes in Fe isotopic composition within the crust[190].

Modeling the potential effect of hydrothermal Fe on the global Fe cycle and surface primary production

The modeling of hydrothermal activity's influence on Fe distribution has primarily concentrated on the long-range transport of Fe, particularly its potential to become bioavailable (e.g., refs. 24,191). However, a few studies focusing on the buoyant and near-field plume have also incorporated a modeling component, such as Neuholz et al.[192], who used radium isotopes to model dispersion.

A main difficulty in modeling the effects of hydrothermalism on Fe distributions has been the parameterization of the strength of the hydrothermal Fe source. Most models follow the approach of Tagliabue et al.[25], which assumed a constant ratio of ^{3}He to Fe release. The release of ^{3}He is – with some caveats—known from models of ^{3}He distribution in the world ocean[193,194], and is thus a readily practicable approach. The proportionality factor needs to be known as well, and was tuned to match the deep-sea distribution of Fe in Tagliabue et al.[25] (see also their Fig. 1 in the supplementary data). This parameterization is roughly equivalent to making the release of Fe proportional to the ridge spreading rate, which is at odds with the known hydrothermal inputs at slowly spreading ridges e.g., in the South Atlantic[23]. Some recent work has further examined the variability of the ^{3}He:Fe ratio for various vent sites[195], so a better parameterization, especially one that considers the pH- and ligand-dependency of Fe loss processes in the plume, might become possible. Local factors such as topography and diapycnal mixing have been proposed to drive the dispersal of DFe from the slow spreading mid Atlantic ridge[196], raising the question how global ocean models in coarse resolution can represent such kind of local processes.

Reversible scavenging has been shown to be important for the far dispersal of hydrothermal Fe[42], and models have started to take these processes into account[45,196,197]. This modeling has suggested that reversible scavenging traps much of the hydrothermal Fe in the deep ocean with only about 3–5% from global hydrothermal vents reaching the surface ocean[197]. On the other hand, trajectory tracking simulations demonstrated that trace metals derived from mid-ocean ridges in the Southern Ocean reach the Southern Ocean surface mixed layer within two decades and may provide micronutrients to fuel the primary production there[29].

An aspect that still needs some further attention in these models is the role of Fe-binding ligands. While most earlier models of the Fe cycle have assumed a spatially and temporally constant organic ligand concentration to reproduce the small inter basin gradient of deep Fe concentrations between Pacific and Atlantic, so far only a limited number of studies have attempted to represent the variability in Fe complexing capacity[174,198,199]. Most models so far, however, do not take sources of ligands from hydrothermalism into account, with the exception of Tagliabue et al.[196]. In this model, the release rate of ligands is set to 50% of the released Fe (note, however, that the Fe release is only the fraction that is not precipitated already in the buoyant plume). Taking ligands into account is made possible by ligands being modeled prognostically, as in Völker and Tagliabue[199], but the prognostic models (as opposed to diagnostic relations between ligands and apparent oxygen utilization and DOC, as used in Misumi et al.[198]) still suffer from uncertainties about the lifetime of ligands, and especially on the role of unspecific binding from DOC[53]. Nevertheless, recent studies have shown that consideration of feedbacks between biological productivity and ligands in models could lead to higher sensitivity of biological responses to changes in external iron supply[200] and drive the system towards iron-macronutrient co-limitation[201]. These studies used ocean box models in different complexity and are motivating further examinations with global models in higher resolution.

New frontiers in hydrothermal Fe, transport, complexation and microbial transformation processes

Our findings build on global perspectives of the marine iron cycle. While Tagliabue et al.[202] highlighted the role of hydrothermal Fe in sustaining the deep-ocean Fe inventory and its shaping ocean biogeochemistry, our work provides the mechanistic basis needed to connect vent-scale Fe speciation, microbial transformations, and organic complexation with large-scale Fe transport and bioavailability. This process-level understanding can improve how hydrothermal Fe sources are represented in ocean biogeochemical models. In contrast to previous modeling-focused assessments, we disentangle the geochemical and biological mechanisms that stabilize Fe, thereby providing the critical process-level constraints to inform and refine future model parameterizations.

Despite significant advances in understanding hydrothermal iron fluxes and their role in ocean biogeochemistry, key challenges and knowledge gaps remain (for a compilation of methods used to study iron in the ocean, please refer to Table 2). An important frontier is targeted sampling across the transitional zones—from buoyant to non-buoyant plumes and from near-field to far-field non-buoyant environments—where transformations in Fe speciation are understudied yet critical for connecting source chemistry and long-range transport. Another major frontier lies in the more systematic characterization of vent fluids, where harmonizing the suite of measured parameters—akin to the GEOTRACES protocol (e.g., ref. 203)—would enable robust comparisons across sites and better integration with plume and non-buoyant plume data. Tracers such as helium, highly effective for tracing fluid origins and transport pathways[204], are still rarely included in standard fluid measurements. Consistent datasets are essential to connect source chemistry to plume transport and transformation processes. A particularly large gap is our limited understanding of the role and magnitude of diffuse hydrothermal inputs, which may contribute substantially to metal budgets but remain poorly constrained. To better link fluid source chemistry with ocean-scale impacts, it would be highly beneficial to compile a comprehensive hydrothermal plume database or to expand existing efforts like MARHYS to include plume chemistry and transport processes. Such a resource would facilitate cross-site comparisons and global-scale flux assessments.

Improved geochemical modeling, especially under high-temperature and high-pressure conditions, is also critical for constraining Fe speciation, kinetics, and complexation. Recent advances in in situ sensors and molecular techniques enable direct observation of iron-bearing nanoparticles, organic ligands, and microbial interactions at the vent source and throughout the water column. However, electrochemical methods commonly used to quantify Fe-binding ligands are increasingly criticized for their inability to distinguish nanoparticulate Fe from ligand-bound dissolved phases[44], limiting our understanding of Fe bioavailability and transport.

While this review has focused on Fe, manganese (Mn)—another redox-active and microbially relevant metal enriched in hydrothermal fluids—deserves greater attention. Like Fe, Mn is an essential micronutrient and plays key roles in microbial metabolism and photosynthesis[205]. Long-range hydrothermal Mn transport has been confirmed[24], but its co-behavior with Fe in plumes appears variable[42], raising questions about whether their transformations are synergistic, independent, or competitive—particularly under shifting conditions of oxygen, pH, and redox.

To advance the field, future research must integrate fluid chemistry, plume processes, microbial transformations, and modeling frameworks across a broader range of hydrothermal environments—including shallow-water systems, submarine groundwater discharge, and cryospheric sources. A deeper understanding of Fe speciation and longevity, and its coupling to biological uptake and export, is essential to predict how hydrothermal iron fluxes respond to climate-driven changes such as ocean warming, acidification, and deoxygenation—and how they ultimately impact ocean productivity and biogeochemical cycles.

https://doi.org/10.1038/s43247-025-02839-4

Table 2 | Method Box

Fraction	Method	Sample prep.	Output	Literature	Notes
Fe_{diss}	ICP-MS[a]	Acid digestion, poss. dilution	Total Fe concentration, ppb to ppt level detection	206	Can simultaneously detect and quantify multiple elements
	ICP-OES[b]	Acid digestion, poss. dilution	Total Fe concentration, ppb level detection	207	Can simultaneously detect multiple elements
	Colorimetric measurement	with Ferrozin or 1,10-Phenanthroline	Fe species, detection limit µM range	207,208	Also applicable for in situ chemical analysis
	DPASV[c]		Fe and Fe species, Fe(II) and Fe(III) are identified and quantified based on their distinct electrochemical signals	209	Suitable for trace levels of Fe species detection
	ICP-MS with speciation techniques		Fe species, extremely high sensitivity and accuracy	183	First separates via e.g., chromatography, detection of species via ICP-MS
	ICP-MS	Acid digestion, maybe dilution	Fe isotopic ratios, Fe concentration range, 0.05-1 nmol L^{-1}	188,210,211	Each Fe isotope produces a distinct peak in the mass spectrum, needs isotopic fractionation correction
$Fe_{NP} + Fe_{rocks}$	TEM/SEM-EDX[d]		Provides spatially resolved elemental analysis down to the nanoscale	151,212	SEM is more suitable for larger sample areas compared to TEM
	XRF[e]		Bulk elemental analysis, for larger quantities of nanoparticles	212	Non-destructive
	SAED[f]		Determination of structures of nanoparticles	213	
	SIMS[g]		Extremely sensitive surface analysis with high spatial resolution	214	
	ICP-MS, -OES, AAS, and colorimetric methods	Acid treatment	Elemental analyses	46,151	Also suitable for digested rocks/sediments/NP
	Mössbauer		Studying Fe speciation (Fe(II) and Fe(III)) and the local environment of Fe atoms in minerals and mineral transformation	215	
	µXRD[h]		Diffraction pattern of X-rays, crystal structure	176	
	µXANES[i]		Oxidation state	216	
	LA-ICP-MS[j]		Micro-scale analysis of Fe distribution and composition within sediments and rocks	217	
Fe_{DOM}	CLE-AdCSV[k]		Complexation of Fe^{3+} with organic ligands	49,183,207,218	Very sensitive
	FT-ICR-MS		Metal-organic complexes	219	
	Purification + NMR		Nanoparticle solid extraction and identification	220	

[a]Inductively coupled plasma mass spectrometry.
[b]Inductively coupled plasma optical emission spectroscopy.
[c]Differential pulse anodic stripping voltammetry.
[d]Transmission electron microscopy/scanning electron microscopy with energy dispersive X-ray spectroscopy.
[e]X-ray fluorescence spectroscopy.
[f]Selected area electron diffraction.
[g]Secondary ion mass spectrometry.
[h]µ-focused X-ray diffraction.
[i]X-ray adsorption near edge structure.
[j]Laser ablation ICP-MS.
[k]Competitive ligand exchange adsorptive stripping voltammetry.

Data availability

The MARHYS data base used to generate the figures is publicly available[54,55]. For this article, no additional datasets were generated.

Received: 27 May 2025; Accepted: 25 September 2025;
Published online: 17 October 2025

References

1. Boyd, P. W. & Ellwood, M. J. The biogeochemical cycle of iron in the ocean. *Nat. Geosci.* **3**, 675–682 (2010).
2. German, C. R., Lang, S. Q. & Fitzsimmons, J. N. Marine hydrothermal processes. In: *Treatise on Geochemistry* 3rd edn (eds Anbar, A. & Weis, D.) (Elsevier, 2025).
3. Williams, R. J. P. The bakerian lecture, 1981 natural selection of the chemical elements. *Proc. R. Soc. Lond. Ser. B Biol. Sci.* **213**, 361–397 (1981).
4. Millero, F. J. Solubility of Fe(III) in seawater. *Earth Planet. Sci. Lett.* **154**, 323–329 (1998).
5. Ruud, J. T. Nitrates and phosphates in the Southern Seas. *ICES J. Mar. Sci.* **5**, 347–360 (1930).
6. Gran, H. H. On the conditions for the production of plankton in the sea. *Cons. Perm. Intern. Pour l'Explor Mer. Rapp. Proces. Verb.* **75**, 37–46 (1931).
7. Hart, T. J. On the phytoplankton of the southeast Atlantic and the Bellingshausen Sea, 1929-1931. *Discov. Rep.* **8**, 1–268 (1934).
8. Bruland, K. W. Oceanographic distributions of cadmium, zinc, nickel, and copper in the North Pacific. *Earth Planet. Sci. Lett.* **47**, 176–198 (1980).
9. Martin, J. H. & Fitzwater, S. E. Iron deficiency limits phytoplankton growth in the north-east Pacific subarctic. *Nature* **331**, 341–343 (1988).
10. Martin, J. H. Glacial-interglacial CO2 change: the iron hypothesis. *Paleoceanography* **5**, 1–13 (1990).
11. Boyd, P. W. et al. Mesoscale iron enrichment experiments 1993-2005: synthesis and future directions. *Science* **315**, 612–617 (2007).
12. Yoon, J.-E. et al. Ocean iron fertilization experiments: past–present–future with introduction to Korean Iron Fertilization Experiment in the Southern Ocean (KIFES) Project. (2016).
13. Moore, J. K., Doney, S. C., Glover, D. M. & Fung, I. Y. Iron cycling and nutrient-limitation patterns in surface waters of the World Ocean. *Deep Sea Res. Part II* **49**, 463–507 (2001).
14. Moore, C. M. et al. Processes and patterns of oceanic nutrient limitation. *Nat. Geosci.* **6**, 701–710 (2013).
15. Browning, T. J. & Moore, C. M. Global analysis of ocean phytoplankton nutrient limitation reveals high prevalence of co-limitation. *Nat. Commun.* **14**, 5014 (2023).
16. Johnson, K. S., Gordon, R. M. & Coale, K. H. What controls dissolved iron concentrations in the world ocean?. *Mar. Chem.* **57**, 137–161 (1997).
17. Archer, D. & Johnson, K. A model of the iron cycle in the ocean. *Glob. Biogeochem. Cycles* **14**, 269–279 (2000).
18. Jickells, T. et al. Global iron connections between desert dust, ocean biogeochemistry, and climate. *science* **308**, 67–71 (2005).
19. Duce, R. A. & Tindale, N. W. Atmospheric transport of iron and its deposition in the ocean. *Limnol. Oceanogr.* **36**, 1715–1726 (1991).
20. Anderson, R. F. & Henderson, G. M. GEOTRACES. *Oceanography* **18**, 76 (2005).
21. Klunder, M., Laan, P., Middag, R., De Baar, H. & Van Ooijen, J. Dissolved iron in the Southern Ocean (Atlantic sector). *Deep Sea Res. Part II* **58**, 2678–2694 (2011).
22. Klunder, M. B. et al. Dissolved iron in the Arctic shelf seas and surface waters of the central Arctic Ocean: impact of Arctic river water and ice-melt. *J. Geophys. Res.* **117**, C01027 (2012).
23. Saito, M. A. et al. Slow-spreading submarine ridges in the South Atlantic as a significant oceanic iron source. *Nat. Geosci.* **6**, 775–779 (2013).
24. Resing, J. A. et al. Basin-scale transport of hydrothermal dissolved metals across the South Pacific Ocean. *Nature* **523**, 200 (2015).
25. Tagliabue, A. et al. Hydrothermal contribution to the oceanic dissolved iron inventory. *Nat. Geosci.* **3**, 252–256 (2010).
26. Schine, C. M. S. et al. Massive Southern Ocean phytoplankton bloom fed by iron of possible hydrothermal origin. *Nat. Commun.* **12**, 1211 (2021).
27. Tagliabue, A. et al. Constraining the contribution of hydrothermal iron to Southern Ocean export production using deep ocean iron observations. *Front. Mar. Sci.* **9**, 754517 (2022).
28. Fourquez, M. et al. Chasing iron bioavailability in the Southern Ocean: insights from Phaeocystis Antarctica and iron speciation. *Sci. Adv.* **9**, eadf9696 (2023).
29. Birchill, A. J. et al. Pathways and timescales of Southern Ocean hydrothermal iron and manganese transport. *Commun. Earth Environ.* **5**, 413 (2024).
30. Elderfield, H. & Schultz, A. Mid-Ocean Ridge hydrothermal fluxes and the chemical composition of the ocean. *Annu. Rev. Earth Planet. Sci.* **24**, 191–224 (1996).
31. Aumont, O., Ethé, C., Tagliabue, A., Bopp, L. & Gehlen, M. PISCES-v2: an ocean biogeochemical model for carbon and ecosystem studies. *Geosci. Model Dev.* **8**, 2465–2513 (2015).
32. Elrod, V. A., Berelson, W. M., Coale, K. H. & Johnson, K. S. The flux of iron from continental shelf sediments: a missing source for global budgets. *Geophys. Res. Lett.* **31**, L12307 (2004).
33. Dale, A. W. et al. A revised global estimate of dissolved iron fluxes from marine sediments. *Glob. Biogeochem. Cycles* **29**, 691–707 (2015).
34. Albani, S. et al. Paleodust variability since the Last Glacial Maximum and implications for iron inputs to the ocean. *Geophys. Res. Lett.* **43**, 3944–3954 (2016).
35. Myriokefalitakis, S. et al. Reviews and syntheses: the GESAMP atmospheric iron deposition model intercomparison study. *Biogeosciences* **15**, 6659–6684 (2018).
36. Raiswell, R. et al. Contributions from glacially derived sediment to the global iron (oxyhydr)oxide cycle: implications for iron delivery to the oceans. *Geochim. Cosmochim. Acta* **70**, 2765–2780 (2006).
37. Chester, R. *Marine Geochemistry* (Springer, 1990).
38. Bennett, S. A. et al. The distribution and stabilisation of dissolved Fe in deep-sea hydrothermal plumes. *Earth Planet. Sci. Lett.* **270**, 157–167 (2008).
39. Radic, A., Lacan, F. & Murray, J. W. Iron isotopes in the seawater of the equatorial Pacific Ocean: New constraints for the oceanic iron cycle. *Earth Planet. Sci. Lett.* **306**, 1–10 (2011).
40. Abadie, C., Lacan, F., Radic, A., Pradoux, C. & Poitrasson, F. Iron isotopes reveal distinct dissolved iron sources and pathways in the intermediate versus deep Southern Ocean. *Proc. Natl. Acad. Sci. USA* **114**, 858–863 (2017).
41. Rudnicki, M. D. & Elderfield, H. A chemical model of the buoyant and neutrally buoyant plume above the TAG vent field, 26 degrees N, Mid-Atlantic Ridge. *Geochim. Cosmochim. Acta* **57**, 2939–2957 (1993).
42. Fitzsimmons, J. N. et al. Iron persistence in a distal hydrothermal plume supported by dissolved-particulate exchange. *Nat. Geosci.* **10**, 195–201 (2017).
43. Gartman, A. & Findlay, A. J. Impacts of hydrothermal plume processes on oceanic metal cycles and transport. *Nat. Geosci.* **13**, 396–402 (2020).
44. Fitzsimmons, J. N. & Steffen, J. M. The "net" impact of hydrothermal venting on oceanic elemental inventories. *Oceanography* **37**, 102–115 (2024).

45. Tagliabue, A. et al. Authigenic mineral phases as a driver of the upper-ocean iron cycle. *Nature* **620**, 104–109 (2023).
46. Yücel, M., Gartman, A., Chan, C. S. & Luther, G. W. Hydrothermal vents as a kinetically stable source of iron-sulphide-bearing nanoparticles to the ocean. *Nat. Geosci.* **4**, 367–371 (2011).
47. Gartman, A., Findlay, A. J. & Luther, G. W. Nanoparticulate pyrite and other nanoparticles are a widespread component of hydrothermal vent black smoker emissions. *Chem. Geol.* **366**, 32–41 (2014).
48. Gartman, A. et al. The role of nanoparticles in mediating element deposition and transport at hydrothermal vents. *Geochim. Cosmochim. Acta* **261**, 113–131 (2019).
49. Sander, S. G. & Koschinsky, A. Metal flux from hydrothermal vents increased by organic complexation. *Nat. Geosci.* **4**, 145–150 (2011).
50. Gledhill, M. & Buck, K. The organic complexation of iron in the marine environment: a review. *Front. Microbiol.* **3**, 69 (2012).
51. Gledhill, M. et al. Trace metal stoichiometry of dissolved organic matter in the Amazon plume. *Sci. Adv.* **8**, eabm2249 (2022).
52. Lodeiro, P. et al. Seasonal variations in proton binding characteristics of dissolved organic matter isolated from the southwest Baltic Sea. *Environ. Sci. Technol.* **55**, 16215–16223 (2021).
53. Lodeiro, P., Rey-Castro, C., David, C., Humphreys, M. P. & Gledhill, M. Proton binding characteristics of dissolved organic matter extracted from the North Atlantic. *Environ. Sci. Technol.* **57**, 21136–21144 (2023).
54. Diehl, A. & Bach, W. MARHYS (MARine HYdrothermal Solutions) Database: a global compilation of marine hydrothermal vent fluid, end member, and seawater compositions. *Geochem. Geophys. Geosyst.* **21**, e2020GC009385 (2020).
55. Diehl, A. & Bach, W. *MARHYS Database 3.0* (PANGAEA, 2023).
56. Syverson, D. D., Awolayo, A. N. & Tutolo, B. M. Seafloor spreading and the delivery of sulfur and metals to Earth's oceans. *Geology* **51**, 1168–1172 (2023).
57. Coumou, D., Driesner, T., Weis, P. & Heinrich, C. A. Phase separation, brine formation, and salinity variation at Black Smoker hydrothermal systems. *J. Geophys. Res.* **114**, B03212 (2009).
58. Edmonds, H. N. & Edmond, J. M. A three-component mixing model for ridge-crest hydrothermal fluids. *Earth Planet. Sci. Lett.* **134**, 53–67 (1995).
59. Kumagai, H. et al. Geological background of the Kairei and Edmond hydrothermal fields along the Central Indian Ridge: implications of their vent fluids' distinct chemistry. *Geofluids* **8**, 239–251 (2008).
60. Albers, E. et al. Ultramafic-influenced submarine venting on basaltic seafloor at the Polaris site, 87° N, Gakkel Ridge. *Earth Planet. Sci. Lett.* **651**, 119166 (2025).
61. Baumberger, T. et al. Constraints on the sedimentary input into the Loki's Castle hydrothermal system (AMOR) from B isotope data. *Chem. Geol.* **443**, 111–120 (2016).
62. Baumberger, T. et al. Fluid composition of the sediment-influenced Loki's Castle vent field at the ultra-slow spreading Arctic Mid-Ocean Ridge. *Geochim. Cosmochim. Acta* **187**, 156–178 (2016).
63. Von Damm, K., Bray, A., Buttermore, L. & Oosting, S. The geochemical controls on vent fluids from the Lucky Strike vent field, Mid-Atlantic Ridge. *Earth Planet. Sci. Lett.* **160**, 521–536 (1998).
64. Von Damm, K. L. Chemistry of hydrothermal vent fluids from 9°–10°N, East Pacific Rise: "Time zero," the immediate posteruptive period. *J. Geophys. Res.* **105**, 11203–11222 (2000).
65. Lowell, R. & Rona, P. Seafloor hydrothermal systems driven by the serpentinization of peridotite. *Geophys. Res. Lett.* **29**, 26-1 (2002).
66. Seyfried, W. Jr, Pester, N. J., Ding, K. & Rough, M. Vent fluid chemistry of the Rainbow hydrothermal system (36 N, MAR): Phase equilibria and in situ pH controls on subseafloor alteration processes. *Geochim. Cosmochim. Acta* **75**, 1574–1593 (2011).
67. Bryce, J., Prado, F. & Von Damm, K. Vent fluid chemistry data, including metals fractions and dissolved majors, from fluid samples acquired with HOV Alvin during Atlantis expedition AT15-13 (2006) at the East Pacific Rise 9N site (System MGD, 2015).
68. Shanks, W., Böhlke, J. K., Seal, R. & Humphris, S. Stable isotopes in mid-ocean ridge hydrothermal systems: Interactions between fluids, minerals, and organisms. *Geophys. Monogr. Am. Geophys. Union* **91**, 194–194 (1995).
69. Lilley, M. D., Butterfield, D. A., Lupton, J. E. & Olson, E. J. Magmatic events can produce rapid changes in hydrothermal vent chemistry. *Nature* **422**, 878–881 (2003).
70. Kleint, C. et al. Geochemical characterization of highly diverse hydrothermal fluids from volcanic vent systems of the Kermadec intraoceanic arc. *Chem. Geol.* **528**, 119289 (2019).
71. Toner, B. M. et al. Preservation of iron(II) by carbon-rich matrices in a hydrothermal plume. *Nat. Geosci.* **2**, 197 (2009).
72. Toner, B. M., German, C. R., Dick, G. J. & Breier, J. A. Deciphering the complex chemistry of deep-ocean particles using complementary synchrotron X-ray microscope and microprobe instruments. *Acc. Chem. Res.* **49**, 128–137 (2016).
73. Noowong, A. et al. Imprint of Kairei and Pelagia deep-sea hydrothermal systems (Indian Ocean) on marine dissolved organic matter. *Org. Geochem.* **152**, 104141 (2021).
74. Sert, M. F. et al. Compositions of dissolved organic matter in the ice-covered waters above the Aurora hydrothermal vent system, Gakkel Ridge, Arctic Ocean. *Biogeosciences* **19**, 2101–2120 (2022).
75. Hawkes, J. A. et al. Efficient removal of recalcitrant deep-ocean dissolved organic matter during hydrothermal circulation. *Nat. Geosci.* **8**, 856–860 (2015).
76. Reeves, E. P., McDermott, J. M., & Seewald, J. S. The origin of methanethiol in midocean ridge hydrothermal fluids. *Proc. Natl. Acad. Sci. USA* **15**, 5474–5479 (2014).
77. Lang, S. Q., Butterfield, D. A., Schulte, M., Kelley, D. S. & Lilley, M. D. Elevated concentrations of formate, acetate and dissolved organic carbon found at the Lost City hydrothermal field. *Geochim. Cosmochim. Acta* **74**, 941–952 (2010).
78. Lang, S. Q. et al. Deeply-sourced formate fuels sulfate reducers but not methanogens at Lost City hydrothermal field. *Sci. Rep.* **8**, 755 (2018).
79. Lollar, B. S. et al. A window into the abiotic carbon cycle–Acetate and formate in fracture waters in 2.7 billion year-old host rocks of the Canadian Shield. *Geochim. Cosmochim. Acta* **294**, 295–314 (2021).
80. Lang, S. Q., Butterfield, D. A., Lilley, M. D., Paul Johnson, H. & Hedges, J. I. Dissolved organic carbon in ridge-axis and ridge-flank hydrothermal systems. *Geochim. Cosmochim. Acta* **70**, 3830–3842 (2006).
81. Butterfield, D. A. et al. Mixing, reaction and microbial activity in the sub-seafloor revealed by temporal and spatial variation in diffuse flow vents at Axial Volcano. In: *The Subseafloor Biosphere at Mid-Ocean Ridges* (eds Wilcock, W. S. D., DeLong, E. F., Kelley, D. S., Baross, J. A. & Cary, S. C.) *Geophysical Monograph* Vol. 144, 269–289 (2004).
82. Pascoe, A. R. & Cann, J. R. Modelling diffuse hydrothermal flow in black smoker vent fields. *Geol. Soc. Lond. Spec. Publ.* **87**, 159–173 (1995).
83. Cooper, M., Elderfield, H. & Schultz, A. Diffuse hydrothermal fluids from Lucky Strike hydrothermal vent field: evidence for a shallow conductively heated system. *J. Geophys. Res.* **105**, 19369–19375 (2000).
84. Lowell, R. P., Crowell, B. W., Lewis, K. C. & Liu, L. Modeling multiphase, multicomponent processes at oceanic spreading centers. *Magma Microbe* **178**, 15–44 (2008).
85. Villinger, H. et al. Evidence for low-temperature diffuse venting at North Pond, western flank of the Mid-Atlantic Ridge. *Geochem. Geophys. Geosyst.* **20**, 2572–2584 (2019).

86. Haase, K. M. et al. Diking, young volcanism and diffuse hydrothermal activity on the southern Mid-Atlantic Ridge: the Lilliput field at 9°33′ S. *Mar. Geol.* **266**, 52–64 (2009).
87. Bemis, K., Lowell, R. P. & Farough, A. Diffuse flow: on and around hydrothermal vents at mid-ocean ridges. *Oceanography* **25**, 182–191 (2012).
88. German, C. R. et al. Hydrothermal Fe cycling and deep ocean organic carbon scavenging: Model-based evidence for significant POC supply to seafloor sediments. *Earth Planet. Sci. Lett.* **419**, 143–153 (2015).
89. Lough, A. J. M. et al. Diffuse hydrothermal venting: a hidden source of iron to the oceans. *Front. Mar. Sci.* **6**, 329 (2019).
90. Fuchida, S., Mizuno, Y., Masuda, H., Toki, T. & Makita, H. Concentrations and distributions of amino acids in black and white smoker fluids at temperatures over 200 °C. *Org. Geochem.* **66**, 98–106 (2014).
91. McCollom, T. M., Seewald, J. S. & German, C. R. Investigation of extractable organic compounds in deep-sea hydrothermal vent fluids along the Mid-Atlantic Ridge. *Geochim. Cosmochim. Acta* **156**, 122–144 (2015).
92. Hansen, C. T. et al. Biodegradability of hydrothermally altered deep-sea dissolved organic matter. *Mar. Chem.* **217**, 103706 (2019).
93. Longnecker, K., Sievert, S. M., Sylva, S. P., Seewald, J. S. & Kujawinski, E. B. Dissolved organic carbon compounds in deep-sea hydrothermal vent fluids from the East Pacific Rise at 9°50′N. *Org. Geochem.* **125**, 41–49 (2018).
94. Rossel, P. E., Stubbins, A., Hach, P. F. & Dittmar, T. Bioavailability and molecular composition of dissolved organic matter from a diffuse hydrothermal system. *Mar. Chem.* **177**, 257–266 (2015).
95. Diehl, A. & Bach, W. The influence of seawater mixing to the element budget at basalt-hosted mid-ocean ridge hydrothermal systems. In *Geophysical Monograph 292, First Edition. Hydrothermal Circulation and Seawater Chemistry: Links and Feedbacks* (eds Coogan, L. A., Turchyn, A. V., Dunlea A. G. & Bach, W.) (AGU, 2026).
96. Liu, X. & Millero, F. J. The solubility of iron hydroxide in sodium chloride solutions. *Geochim. Cosmochim. Acta* **63**, 3487–3497 (1999).
97. Rickard, D. The solubility of FeS. *Geochim. Cosmochim. Acta* **70**, 5779–5789 (2006).
98. Breier, J. et al. Sulfur, sulfides, oxides and organic matter aggregated in submarine hydrothermal plumes at 9°50′ N East Pacific Rise. *Geochim. Cosmochim. Acta* **88**, 216–236 (2012).
99. Bryce, J., Prado, F. & Von Damm, K. Vent fluid chemistry data, including metals fractions and dissolved majors, from fluid samples acquired with HOV Alvin during Atlantis Expedition AT15-13 (2006) at the East Pacific Rise 9N Site (IEDA, 2015).
100. Yücel, M., Sevgen, S. & Le Bris, N. Soluble, colloidal, and particulate iron across the hydrothermal vent mixing zones in broken spur and Rainbow, Mid-Atlantic Ridge. *Front. Microbiol.* **12**, 631885 (2021).
101. Mottl, M. J. & McConachy, T. F. Chemical processes in buoyant hydrothermal plumes on the East Pacific Rise near 21°N. *Geochim. Cosmochim. Acta* **54**, 1911–1927 (1990).
102. Field, M. P. & Sherrell, R. M. Dissolved and particulate Fe in a hydrothermal plume at 9°45′ N, East Pacific Rise:: slow Fe (II) oxidation kinetics in Pacific plumes. *Geochim. Cosmochim. Acta* **64**, 619–628 (2000).
103. Severmann, S. et al. The effect of plume processes on the Fe isotope composition of hydrothermally derived Fe in the deep ocean as inferred from the Rainbow vent site, Mid-Atlantic Ridge, 36°14′N. *Earth Planet. Sci. Lett.* **225**, 63–76 (2004).
104. Sevgen, S., Le Bris, N. & Yücel, M. The control of end-member iron-to-sulfide ratios on hydrothermal plume geochemistry at the Rainbow, broken spur, and Lost City vent fields in the Mid-Atlantic Ridge. *Geochem. Geophys. Geosyst.* **26**, e2025GC012370 (2025).
105. Zeng, X., Alain, K. & Shao, Z. Microorganisms from deep-sea hydrothermal vents. *Mar. Life Sci. Technol.* **3**, 204–230 (2021).
106. Weber, K. A., Achenbach, L. A. & Coates, J. D. Microorganisms pumping iron: anaerobic microbial iron oxidation and reduction. *Nat. Rev. Microbiol.* **4**, 752–764 (2006).
107. Makita, H. Iron-oxidizing bacteria in marine environments: recent progresses and future directions. *World J. Microbiol. Biotechnol.* **34**, 110 (2018).
108. Lovley, D. R. Dissimilatory Fe (III) and Mn (IV) reduction. *Microbiol. Rev.* **55**, 259–287 (1991).
109. Han, Y. et al. Hydrothermal chimneys host habitat-specific microbial communities: analogues for studying the possible impact of mining seafloor massive sulfide deposits. *Sci. Rep.* **8**, 10386 (2018).
110. Slobodkin, A., Campbell, B., Cary, S. C., Bonch-Osmolovskaya, E. & Jeanthon, C. Evidence for the presence of thermophilic Fe(III)-reducing microorganisms in deep-sea hydrothermal vents at 13°N (East Pacific Rise). *FEMS Microbiol. Ecol.* **36**, 235–243 (2001).
111. Slobodkina, G. et al. Deferrisoma camini gen. nov., sp. nov., a moderately thermophilic, dissimilatory iron (III)-reducing bacterium from a deep-sea hydrothermal vent that forms a distinct phylogenetic branch in the Deltaproteobacteria. *Int. J. Syst. Evolut. Microbiol.* **62**, 2463–2468 (2012).
112. Miroshnichenko, M. et al. Deferribacter abyssi sp. nov., an anaerobic thermophile from deep-sea hydrothermal vents of the Mid-Atlantic Ridge. *Int. J. Syst. Evolut. Microbiol.* **53**, 1637–1641 (2003).
113. Kashyap, S., Musa, M., Neat, K. A., Leopo, D. A. & Holden, J. F. Desulfovulcanus ferrireducens gen. nov., sp. nov., a thermophilic autotrophic iron and sulfate-reducing bacterium from subseafloor basalt that grows on akaganéite and lepidocrocite minerals. *Extremophiles* **26**, 13 (2022).
114. Zeng, X. et al. Caloranaerobacter ferrireducens sp. nov., an anaerobic, thermophilic, iron (III)-reducing bacterium isolated from deep-sea hydrothermal sulfide deposits. *Int. J. Syst. Evolut. Microbiol.* **65**, 1714–1718 (2015).
115. Chen, Y. et al. Thermosipho ferrireducens sp. nov., an anaerobic thermophilic iron (III)-reducing bacterium isolated from a deep-sea hydrothermal sulfide deposits. *Int. J. Syst. Evolut. Microbiol.* **71**, 004929 (2021).
116. Pérez-Rodríguez, I., Rawls, M., Coykendall, D. K. & Foustoukos, D. I. Deferrisoma palaeochoriense sp. nov., a thermophilic, iron(III)-reducing bacterium from a shallow-water hydrothermal vent in the Mediterranean Sea. *Int. J. Syst. Evolut. Microbiol.* **66**, 830–836 (2016).
117. Lim, J. K. et al. Thermococcus indicus sp. nov., a Fe (III)-reducing hyperthermophilic archaeon isolated from the Onnuri Vent Field of the Central Indian Ocean ridge. *J. Microbiol.* **58**, 260–267 (2020).
118. Kashefi, K., Holmes, D. E., Baross, J. A. & Lovley, D. R. Thermophily in the Geobacteraceae: Geothermobacter ehrlichii gen. nov., sp. nov., a novel thermophilic member of the Geobacteraceae from the “Bag City” hydrothermal vent. *Appl. Environ. Microbiol.* **69**, 2985–2993 (2003).
119. Reysenbach, A.-L. et al. A ubiquitous thermoacidophilic archaeon from deep-sea hydrothermal vents. *Nature* **442**, 444–447 (2006).
120. Roh, Y. et al. Metal reduction and iron biomineralization by a psychrotolerant Fe (III)-reducing bacterium, Shewanella waksmanii, isolated from microbial mat at Naha Hydrothermal Vent, Loihi Seamount, Hawaii. *Appl. Environ. Microbiol.* **72**, 3236–3244 (2004).
121. Uroz, S., Kelly, L. C., Turpault, M.-P., Lepleux, C. & Frey-Klett, P. The mineralosphere concept: mineralogical control of the distribution and function of mineral-associated bacterial communities. *Trends Microbiol.* **23**, 751–762 (2015).
122. Kashefi, K. & Lovley, D. R. Extending the upper temperature limit for life. *Science* **301**, 934–934 (2003).

123. Takai, K. et al. Cell proliferation at 122 °C and isotopically heavy CH_4 production by a hyperthermophilic methanogen under high-pressure cultivation. *Proc. Natl. Acad. Sci. USA* **105**, 10949–10954 (2008).
124. He, Y., Zeng, X., Xu, F. & Shao, Z. Diversity of mixotrophic neutrophilic thiosulfate-and iron-oxidizing bacteria from deep-sea hydrothermal vents. *Microorganisms* **11**, 100 (2022).
125. Edwards, K. J., Rogers, D. R., Wirsen, C. O. & McCollom, T. Isolation and characterization of novel psychrophilic, neutrophilic, Fe-oxidizing, chemolithoautotrophic α-and γ-Proteobacteria from the deep sea. *Appl. Environ. Microbiol.* **69**, 2906–2913 (2003).
126. Vander Roost, J., Daae, F. L., Steen, I. H., Thorseth, I. H. & Dahle, H. Distribution patterns of iron-oxidizing Zeta-and Beta-proteobacteria from different environmental settings at the Jan Mayen Vent fields. *Front. Microbiol.* **9**, 3008 (2018).
127. Handley, K. M. & Lloyd, J. R. Biogeochemical implications of the ubiquitous colonization of marine habitats and redox gradients by Marinobacter species. *Front. Microbiol.* **4**, 136 (2013).
128. Laufer-Meiser, K. et al. Oxidation of sulfur, hydrogen, and iron by metabolically versatile Hydrogenovibrio from deep sea hydrothermal vents. *ISME J.* **18**, wrae173 (2024).
129. McAllister, S. M., Vandzura, R., Keffer, J. L., Polson, S. W. & Chan, C. S. Aerobic and anaerobic iron oxidizers together drive denitrification and carbon cycling at marine iron-rich hydrothermal vents. *ISME J.* **15**, 1271–1286 (2021).
130. Astorch-Cardona, A. et al. Linking Zetaproteobacterial diversity and substratum type in iron-rich microbial mats from the Lucky Strike hydrothermal field (EMSO-Azores observatory). *Appl. Environ. Microbiol.* **90**, e02041–02023 (2024).
131. Emerson, D. & Moyer, C. L. Neutrophilic Fe-oxidizing bacteria are abundant at the Loihi Seamount hydrothermal vents and play a major role in Fe oxide deposition. *Appl. Environ. Microbiol.* **68**, 3085–3093 (2002).
132. Emerson, D. et al. A novel lineage of proteobacteria involved in formation of marine Fe-oxidizing microbial mat communities. *PLoS ONE* **2**, e667 (2007).
133. Chan, C. S., Fakra, S. C., Emerson, D., Fleming, E. J. & Edwards, K. J. Lithotrophic iron-oxidizing bacteria produce organic stalks to control mineral growth: implications for biosignature formation. *ISME J.* **5**, 717–727 (2010).
134. Hribovšek, P. et al. Putative novel hydrogen- and iron-oxidizing sheath-producing Zetaproteobacteria thrive at the Fåvne deep-sea hydrothermal vent field. *mSystems* **8**, e00543–00523 (2023).
135. Makita, H. et al. Comparative analysis of microbial communities in iron-dominated flocculent mats in deep-sea hydrothermal environments. *Appl. Environ. Microbiol.* **82**, 5741–5755 (2016).
136. Van der Zwan, F. M. et al. Widespread diffuse venting and large microbial iron-mounds in the Red Sea. *Commun. Earth Environ.* **4**, 496 (2023).
137. Astorch-Cardona, A., Guerre, M., Dolla, A., Chavagnac, V. & Rommevaux, C. Spatial comparison and temporal evolution of two marine iron-rich microbial mats from the lucky strike hydrothermal field, related to environmental variations. *Front. Mar. Sci.* **10**, 1038192 (2023).
138. Böhnke, S. & Perner, M. Seeking active RubisCOs from the currently uncultured microbial majority colonizing deep-sea hydrothermal vent environments. *ISME J.* **13**, 2475–2488 (2019).
139. Barco, R. A. et al. In-situ incubation of iron-sulfur mineral reveals a diverse chemolithoautotrophic community and a new biogeochemical role for Thiomicrospira. *Environ. Microbiol* **19**, 1322–1337 (2017).
140. Neely, C. et al. Genome sequence of Hydrogenovibrio sp. strain SC-1, a chemolithoautotrophic sulfur and iron oxidizer. *Genome Announc.* **6**, 01581–01517 (2018).
141. Nakagawa, S. et al. Deep-sea vent ε-proteobacterial genomes provide insights into emergence of pathogens. *Proc. Natl. Acad. Sci. USA* **104**, 12146–12150 (2007).
142. Baker, E. et al. Episodic venting of hydrothermal fluids from the Juan de Fuca Ridge. *J. Geophys. Res. Solid Earth* **94**, 9237–9250 (1989).
143. German, C. R., Campbell, A. C. & Edmond, J. M. Hydrothermal scavenging at the Mid-Atlantic Ridge: modification of trace element dissolved fluxes. *Earth Planet. Sci. Lett.* **107**, 101–114 (1991).
144. Lough, A. J. M. et al. Soluble iron conservation and colloidal iron dynamics in a hydrothermal plume. *Chem. Geol.* **511**, 225–237 (2019).
145. Seyfried, W. E. & Ding, K. The hydrothermal chemistry of fluoride in seawater. *Geochim. Cosmochim. Acta* **59**, 1063–1071 (1995).
146. Rickard, D. Kinetics of FeS precipitation: Part 1. Competing reaction mechanisms. *Geochim. Cosmochim. Acta* **59**, 4367–4379 (1995).
147. Waeles, M. et al. On the early fate of hydrothermal iron at deep-sea vents: a reassessment after in situ filtration. *Geophys. Res. Lett.* **44**, 4233–4240 (2017).
148. Findlay, A. J., Gartman, A., Shaw, T. J. & Luther, G. W. Trace metal concentration and partitioning in the first 1.5m of hydrothermal vent plumes along the Mid-Atlantic Ridge: TAG, Snakepit, and Rainbow. *Chem. Geol.* **412**, 117–131 (2015).
149. Feely, R. A. et al. Composition and dissolution of black smoker particulates from active vents on the Juan de Fuca Ridge. *J. Geophys. Res. Solid Earth* **92**, 11347–11363 (1987).
150. Speer, K. G. & Rona, P. A. A model of an Atlantic and Pacific hydrothermal plume. *J. Geophys. Res. Oceans* **94**, 6213–6220 (1989).
151. Findlay, A. J. et al. Iron and sulfide nanoparticle formation and transport in nascent hydrothermal vent plumes. *Nat. Commun.* **10**, 1597 (2019).
152. Rozan, T. F., Lassman, M. E., Ridge, D. P. & Luther, G. W. Evidence for iron, copper and zinc complexation as multinuclear sulphide clusters in oxic rivers. *Nature* **406**, 879–882 (2000).
153. Luther, G. W. & Rickard, D. T. Metal sulfide cluster complexes and their biogeochemical importance in the environment. *J. Nanopart. Res.* **7**, 389–407 (2005).
154. Findlay A. J. *Sulfide Oxidation and (Nano) Particle Formation Along Redox Gradients in The Marine Environment* (University of Delaware, 2015).
155. Tilliette, C. et al. Dissolved iron patterns impacted by shallow hydrothermal sources along a transect through the Tonga-Kermadec arc. *Glob. Biogeochem. Cycles* **36**, e2022GB007363 (2022).
156. Mahieu, L. et al. Iron-binding by dissolved organic matter in the Western Tropical South Pacific Ocean (GEOTRACES TONGA cruise GPpr14). *Front. Mar. Sci.* **11**, 1304118 (2024).
157. Kleint, C., Hawkes, J. A., Sander, S. G. & Koschinsky, A. Voltammetric investigation of hydrothermal iron speciation. *Front. Mar. Sci.* **3**, 75 (2016).
158. Wang, H. et al. The characteristics of Fe speciation and Fe-binding ligands in the Mariana back-arc hydrothermal plumes. *Geochim. Cosmochim. Acta* **292**, 24–36 (2021).
159. Li, M. et al. Microbial iron uptake as a mechanism for dispersing iron from deep-sea hydrothermal vents. *Nat. Commun.* **5**, 3192 (2014).
160. Bennett, S. A., Hansman, R. L., Sessions, A. L., Nakamura, K. -i & Edwards, K. J. Tracing iron-fueled microbial carbon production within the hydrothermal plume at the Loihi seamount. *Geochim. Cosmochim. Acta* **75**, 5526–5539 (2011).
161. Holden, J. F. & Adams, M. W. W. Microbe-metal interactions in marine hydrothermal environments. *Curr. Opin. Chem. Biol.* **7**, 160–165 (2003).
162. Fullerton, H. et al. Seafloor incubation experiments at deep-sea hydrothermal vents reveal distinct biogeographic signatures of

autotrophic communities. *FEMS Microbiol. Ecol.* **100**, fiae001 (2024).
163. Hansen, C. T. et al. Impact of high Fe-concentrations on microbial community structure and dissolved organics in hydrothermal plumes: an experimental study. *Sci. Rep.* **12**, 20723 (2022).
164. Perner, M. et al. Linking geology, fluid chemistry, and microbial activity of basalt- and ultramafic-hosted deep-sea hydrothermal vent environments. *Geobiology* **11**, 340–355 (2013).
165. Han, Y. & Perner, M. The globally widespread genus Sulfurimonas: versatile energy metabolisms and adaptations to redox clines. *Front. Microbiol.* **6**, 989 (2015).
166. Lesniewski, R. A., Jain, S., Anantharaman, K., Schloss, P. D. & Dick, G. J. The metatranscriptome of a deep-sea hydrothermal plume is dominated by water column methanotrophs and lithotrophs. *ISME J.* **6**, 2257–2268 (2012).
167. Henkel, J. V. et al. Candidatus Sulfurimonas marisnigri sp. nov. and Candidatus Sulfurimonas baltica sp. nov., thiotrophic manganese oxide reducing chemolithoautotrophs of the class Campylobacteria isolated from the pelagic redoxclines of the Black Sea and the Baltic Sea. *Syst. Appl. Microbiol.* **44**, 126155 (2021).
168. Dede, B. et al. Niche differentiation of sulfur-oxidizing bacteria (SUP05) in submarine hydrothermal plumes. *ISME J.* **16**, 1479–1490 (2022).
169. Fang, Z. & Wang, W.-X. Size speciation of dissolved trace metals in hydrothermal plumes on the Southwest Indian Ridge. *Sci. Total Environ.* **771**, 145367 (2021).
170. Carazzo, G., Jellinek, A. M. & Turchyn, A. V. The remarkable longevity of submarine plumes: implications for the hydrothermal input of iron to the deep-ocean. *Earth Planet. Sci. Lett.* **382**, 66–76 (2013).
171. German, C. R. et al. Hydrothermal impacts on trace element and isotope ocean biogeochemistry. *Philos. Trans. R. Soc. A Math. Phys. Eng. Sci.* **374**, 20160035 (2016).
172. Wu, J., Wells, M. L. & Rember, R. Dissolved iron anomaly in the deep tropical–subtropical Pacific: evidence for long-range transport of hydrothermal iron. *Geochim. Cosmochim. Acta* **75**, 460–468 (2011).
173. González-Santana, D. et al. Processes driving iron and manganese dispersal from the TAG hydrothermal plume (Mid-Atlantic Ridge): results from a GEOTRACES process study. *Front. Mar. Sci.* **7**, 568 (2020).
174. Ye, Y., Völker, C. & Gledhill, M. Exploring the iron-binding potential of the ocean using a combined pH and DOC parameterization. *Glob. Biogeochem. Cycles* **34**, e2019GB006425 (2020).
175. Statham, P. J., German, C. R. & Connelly, D. P. Iron (II) distribution and oxidation kinetics in hydrothermal plumes at the Kairei and Edmond vent sites, Indian Ocean. *Earth Planet. Sci. Lett.* **236**, 588–596 (2005).
176. Toner, B. M. et al. Biogenic iron oxyhydroxide formation at mid-ocean ridge hydrothermal vents: Juan de Fuca Ridge. *Geochim. Cosmochim. Acta* **73**, 388–403 (2009).
177. Hawkes, J. A., Connelly, D. P., Gledhill, M. & Achterberg, E. P. The stabilisation and transportation of dissolved iron from high temperature hydrothermal vent systems. *Earth Planet. Sci. Lett.* **375**, 280–290 (2013).
178. Dulaquais, G. et al. The role of humic-type ligands in the bioavailability and stabilization of dissolved iron in the Western Tropical South Pacific Ocean. *Front. Mar. Sci.* **10**, 1219594. (2023).
179. Tagliabue, A. et al. Surface-water iron supplies in the Southern Ocean sustained by deep winter mixing. *Nat. Geosci.* **7**, 314–320 (2014).
180. Maak, J. M. et al. The energy-efficient reductive tricarboxylic acid cycle drives carbon uptake and transfer to higher trophic levels within the Kueishantao shallow-water hydrothermal system. *Biogeosciences* **22**, 1853–1863 (2025).
181. Hoffman, C. L. et al. Near-field iron and carbon chemistry of non-buoyant hydrothermal plume particles, Southern East Pacific Rise 15 S. *Mar. Chem.* **201**, 183–197 (2018).
182. Hoffman, C. L. et al. Microbial strong organic-ligand production is tightly coupled to iron in hydrothermal plumes. *Biogeosciences* **21**, 5233–5246 (2024).
183. Wang, H. et al. Iron ligands and isotopes in hydrothermal plumes over backarc volcanoes in the Northeast Lau Basin, Southwest Pacific Ocean. *Geochim. Cosmochim. Acta* **336**, 341–352 (2022).
184. Rouxel, O., Shanks, W. C. III, Bach, W. & Edwards, K. J. Integrated Fe-and S-isotope study of seafloor hydrothermal vents at East Pacific Rise 9–10 N. *Chem. Geol.* **252**, 214–227 (2008).
185. Sharma, M., Polizzotto, M. & Anbar, A. Iron isotopes in hot springs along the Juan de Fuca Ridge. *Earth Planet. Sci. Lett.* **194**, 39–51 (2001).
186. Beard, B. L., Johnson, C. M., Von Damm, K. L. & Poulson, R. L. Iron isotope constraints on Fe cycling and mass balance in oxygenated Earth oceans. *Geology* **31**, 629–632 (2003).
187. Severmann, S., Johnson, C. M., Beard, B. L. & McManus, J. The effect of early diagenesis on the Fe isotope compositions of porewaters and authigenic minerals in continental margin sediments. *Geochim. Cosmochim. Acta* **70**, 2006–2022 (2006).
188. Nasemann, P., Gault-Ringold, M., Stirling, C. H., Koschinsky, A. & Sander, S. G. Processes affecting the isotopic composition of dissolved iron in hydrothermal plumes: a case study from the Vanuatu back-arc. *Chem. Geol.* **476**, 70–84 (2018).
189. Bennett, S. A. et al. Iron isotope fractionation in a buoyant hydrothermal plume, 5°S Mid-Atlantic Ridge. *Geochim. Cosmochim. Acta* **73**, 5619–5634 (2009).
190. Chu, N.-C. et al. Evidence for hydrothermal venting in Fe isotope compositions of the deep Pacific Ocean through time. *Earth Planet. Sci. Lett.* **245**, 202–217 (2006).
191. Ardyna, M. et al. Hydrothermal vents trigger massive phytoplankton blooms in the Southern Ocean. *Nat. Commun.* **10**, 2451 (2019).
192. Neuholz, R. et al. Near-field hydrothermal plume dynamics at Brothers Volcano (Kermadec Arc): a short-lived radium isotope study. *Chem. Geol.* **533**, 119379 (2020).
193. Farley, K., Maier-Reimer, E., Schlosser, P. & Broecker, W. Constraints on mantle 3He fluxes and deep-sea circulation from an oceanic general circulation model. *J. Geophys. Res. Solid Earth* **100**, 3829–3839 (1995).
194. Dutay, J.-C. et al. Evaluation of OCMIP-2 ocean models' deep circulation with mantle helium-3. *J. Mar. Syst.* **48**, 15–36 (2004).
195. Lough, A. J. et al. Tracing differences in iron supply to the Mid-Atlantic Ridge valley between hydrothermal vent sites: implications for the addition of iron to the deep ocean. *Biogeosciences* **20**, 405–420 (2023).
196. Tagliabue, A. et al. Mechanisms driving the dispersal of hydrothermal iron from the Northern Mid Atlantic Ridge. *Geophys. Res. Lett.* **49**, e2022GL100615 (2022).
197. Roshan, S., DeVries, T., Wu, J., John, S. & Weber, T. Reversible scavenging traps hydrothermal iron in the deep ocean. *Earth Planet. Sci. Lett.* **542**, 116297 (2020).
198. Misumi, K. et al. Humic substances may control dissolved iron distributions in the global ocean: Implications from numerical simulations. *Glob. Biogeochem. Cycles* **27**, 450–462 (2013).
199. Völker, C. & Tagliabue, A. Modeling organic iron-binding ligands in a three-dimensional biogeochemical ocean model. *Mar. Chem.* **173**, 67–77 (2015).
200. Völker, C. & Ye, Y. Feedbacks between ocean productivity and organic iron complexation in reaction to changes in ocean iron supply. *Front. Mar. Sci.* **9**, 777334 (2022).
201. Lauderdale, J. M., Braakman, R., Forget, G., Dutkiewicz, S. & Follows, M. J. Microbial feedbacks optimize ocean iron availability. *Proc. Natl. Acad. Sci. USA* **117**, 4842–4849 (2020).

202. Tagliabue, A. et al. The integral role of iron in ocean biogeochemistry. *Nature* **543**, 51–59 (2017).
203. Anderson, R. F., Mawji, E., Cutter, G. A., Measures, C. I. & Jeandel, C. GEOTRACES: changing the way we explore ocean chemistry. *Oceanography* **27**, 50–61 (2014).
204. Lupton, J. Hydrothermal helium plumes in the Pacific Ocean. *J. Geophys. Res.* **103**, 15853–15868 (1998).
205. Tebo, B. M. et al. Biogenic manganese oxides: properties and mechanisms of formation. *Annu Rev. Earth Planet Sci.* **32**, 287–328 (2004).
206. Schmidt, K. et al. Boiling vapour-type fluids from the Nifonea vent field (New Hebrides Back-Arc, Vanuatu, SW Pacific): Geochemistry of an early-stage, post-eruptive hydrothermal system. *Geochim. Cosmochim. Acta* **207**, 185–209 (2017).
207. Kleint, C., Pichler, T. & Koschinsky, A. Geochemical characteristics, speciation and size-fractionation of iron (Fe) in two marine shallow-water hydrothermal systems, Dominica, Lesser Antilles. *Chem. Geol.* **454**, 44–53 (2017).
208. Sarradin, P.-M., Le, B. N., Le, G. C. & Rodier, P. Fe analysis by the ferrozine method: Adaptation to FIA towards in situ analysis in hydrothermal environment. *Talanta* **66**, 1131–1138 (2005).
209. Mikkelsen, Ø, van den Berg, C. M. G. & Schrøder, K. H. Determination of labile iron at low nmol L−1 levels in estuarine and coastal waters by anodic stripping voltammetry. *Electroanalysis* **18**, 35–43 (2006).
210. Lacan, F. et al. High-precision determination of the isotopic composition of dissolved iron in iron depleted seawater by double spike multicollector-ICPMS. *Anal. Chem.* **82**, 7103–7111 (2010).
211. Klar, J. K. et al. Isotopic signature of dissolved iron delivered to the Southern Ocean from hydrothermal vents in the East Scotia Sea. *Geology* **45**, 351–354 (2017).
212. von der Heyden, B., Roychoudhury, A. & Myneni, S. Iron-rich nanoparticles in natural aquatic environments. *Minerals* **9**, 287 (2019).
213. Ponce, A., Aguilar, J. A., Tate, J. & Yacamán, M. J. Advances in the electron diffraction characterization of atomic clusters and nanoparticles. *Nanoscale Adv.* **3**, 311–325 (2021).
214. Hultquist, G., Seo, M., Lu, Q., Chuah, G. K. & Tan, K. L. Surface reactions at 300–750 K in the iron-oxygen-water system studied by SIMS. *Appl. Surf. Sci.* **59**, 135–145 (1992).
215. Notini, L. et al. A new approach for investigating iron mineral transformations in soils and sediments using ^{57}Fe-labeled minerals and ^{57}Fe Mössbauer spectroscopy. *Environ. Sci. Technol.* **57**, 10008–10018 (2023).
216. Sundman, A., Karlsson, T., Laudon, H. & Persson, P. XAS study of iron speciation in soils and waters from a boreal catchment. *Chem. Geol.* **364**, 93–102 (2014).
217. Cook, N. et al. Trace element analysis of minerals in magmatic-hydrothermal ores by laser ablation inductively-coupled plasma mass spectrometry: approaches and opportunities. *Minerals* **6**, 111 (2016).
218. Abualhaija, M. M. & van den Berg, C. M. G. Chemical speciation of iron in seawater using catalytic cathodic stripping voltammetry with ligand competition against salicylaldoxime. *Mar. Chem.* **164**, 60–74 (2014).
219. Waska H., Koschinsky A. & Dittmar T. Fe- and Cu-complex formation with artificial ligands investigated by ultra-high resolution fourier-transform ion cyclotron resonance mass spectrometry (FT-ICR-MS): implications for natural metal-organic complex studies. *Front. Mar. Sci.* **3**, 119 (2016).
220. Egbers, P. H., Harder, T., Koch, B. P. & Tebben, J. Siderophore purification with titanium dioxide nanoparticle solid phase extraction. *Analyst* **145**, 7303–7311 (2020).

Acknowledgements

A.D. was funded by the German Research Foundation (DFG) under Germany's Excellence Strategy—EXC-2077-The Ocean Floor Earth's Uncharted Interface— 390741603 and Y.Y. was supported by a DFG project (Grant YE 170/2-1).

Author contributions

S.I.B., S.B.-B., A.D., M.G., L.H., C.K., A.K., S.L., M.P., S.G.S., C.V., and Y.Y. contributed to literature survey writing and revising the manuscript. A.D. extracted, filtered, and analyzed vent fluid data, M.G. analyzed vent fluid data statistics, and L.H. performed solubility modeling. S.I.B., S.B.-B., A.D., and M.G. contributed to visualization and figure preparation.

Funding

Open Access funding enabled and organized by Projekt DEAL.

Competing interests

The authors declare no competing interests.

Additional information

Supplementary information The online version contains supplementary material available at https://doi.org/10.1038/s43247-025-02839-4.

Correspondence and requests for materials should be addressed to Solveig I. Bühring.

Peer review information *Communications Earth and Environment* thanks Zenghui Yu, Guy Evans, and the other anonymous reviewer(s) for their contribution to the peer review of this work. Primary handling editors: D'Arcy Meyer-Dombard and Alice Drinkwater. A peer review file is available.